Original Article

Vehicle tip-over prevention using gain-scheduled State-dependent Riccati Equation–based anti-rollover controller

Hari M Nair(iD) and C Sujatha

Abstract
The most hazardous kind of vehicle crash among all road accidents is vehicle rollover. Present-day rollover prevention systems in commercial vehicles mitigate rollover by preventing any wheel lift-off from the ground. These systems make use of actuators such as differential brakes and demand all the wheels on the ground for satisfactory operation. Such systems are not effective in recovering a vehicle from intense rollover scenarios where the wheels on one side are lifted off the ground, and the vehicle is about to rollover to the other side after reaching the tip-over point. A few studies have investigated the possibility of reinstating a vehicle at the tip-over point with the wheels on a side lifted off. The high complexity and computation time of the optimal control strategies such as nonlinear model predictive controller make it unsuitable for real-time implementations. This study proposes a novel gain-scheduled State-dependent Riccati Equation–based optimal anti-rollover controller for reinstating a vehicle from the tip-over point. An inverted double pendulum on a cart vehicle model is used as the plant model. The anti-rollover controller is found to be presentable as a two-dimensional gain-scheduled lookup table with specific state dependencies in existence. It eliminates the necessity of solving the nonlinear performance index minimization problem online. State-dependent Riccati Equation method adequately accounts for the nonlinearities involved, yet possesses a small computational time per sample. The anti-rollover controller is evaluated with a 10 degrees of freedom full vehicle model with a nonlinear pure slip tyre model that incorporates the dynamical effects neglected in the controller formulation. Finally, the anti-rollover controller is evaluated in real-life initial conditions using a sophisticated pick-up truck model obtained from TruckSim® software through a co-simulation with the anti-rollover controller setup in MATLAB®/Simulink® environment. The State-dependent Riccati Equation controller was found to be effective in reinstating the higher-order models from the tip-over point in all the case studies conducted.

Introduction

Rollover is the most hazardous kind of vehicle crash and has the highest fatality rate compared to other road vehicle accidents. In India, vehicle rollovers claimed more than 9000 lives in the year 2017.[1] Every year, rollover crashes kill more than 10,000 people in the United States.[2] Vehicle rollovers occur in two categories based on the cause of the wheel lift-off: tripped rollovers and untripped rollovers. In tripped rollovers, the wheel lift-off occurs due to external tripping forces which act on the vehicle as it encounters an obstacle such as a guard rail or bump. On the contrary, in untripped rollovers, the wheel lift-off occurs due to the generation of a high inertial roll moment about the roll axis during events such as high-speed collision avoidance manoeuvre.

A vehicle anti-rollover system comprises rollover prediction and prevention systems, for which, a remarkable body of work exists in literature. A rollover prediction system monitors the vehicle in real-time for any potential wheel lift-off through the indirect estimation of normal reaction forces on tyres. The rollover index (RI) has been the most common parameter used for the indication of the vehicle's roll state.[3–5] Roll energy of the vehicle is another parameter used to analyse as well

Indian Institute of Technology Madras, Chennai, India

Corresponding author:
Hari M Nair, Department of Mechanical Engineering, Indian Institute of Technology Madras, Chennai 600036, India.
Email: harinairm@gmail.com

as predict the roll state of the vehicle.[6] In the event of a wheel lift-off, the rollover prediction system sends out a warning, and the rollover prevention system contains the impending rollover scenario. Researchers have proposed various rollover prevention systems in which actuators such as active torque distributors, differential brakes, active suspension, active anti-roll bars and active steering were in use. The most common actuators in use among these are differential brakes and active torque distributors who use the brake force and driving torque, respectively, to control the yaw motion of the vehicle, which in turn controls the roll motion.[7,8] Direct control of roll motion exists in active suspensions, active steering and active anti-roll bars.[9–11] It is evident that in all the rollover prevention systems mentioned before, the system achieved the containment of a potential rollover scenario by avoiding any possible wheel lift-off from the ground. Hence, these anti-rollover systems are sensitive only at the wheel lift-off point. Once the wheels on any side lifts off, the most common differential braking and active torque distributor control are not fully functional, with only two wheels on the ground.

It is known that a timely involvement of an effective rollover prevention system can safely bring back a vehicle, even after a wheel lift-off has occurred. An inverted double pendulum on a massless cart (IDPC) model can be used to present the dynamics of a four-wheeled vehicle at a tip-over point.[12] The number of degrees of freedom (DOF) of the nonlinear IDPC vehicle model is higher than that of the inputs. Hence, the system can be termed as underactuated. Nonlinear controllers like nonlinear model predictive controller (NMPC) have found their use along with the IDPC vehicle model to control a vehicle in tip-over scenario.[13,14] In the beginning, the energy-based nonlinear controllers found their applications in lifting up an IDPC model from any initial condition for the subsequent settlement in the upright position.[15–17] Later on, the energy-based controller was used along with the IDPC model for reinstating a vehicle from tip-over point.[18] The NMPC controller is effective, but highly complicated and demands high computational effort per sample. The energy-based controller, on the contrary, is simple but shows slow responsiveness and requires additional controllers to achieve effectiveness in control action.

The State-dependent Riccati equation (SDRE) method is a nonlinear extension of the linear quadratic regulator (LQR) method and is well suited for highly nonlinear control problems. The effectiveness of the SDRE-based optimal vehicle dynamics control strategy has been experimentally validated.[19] SDRE controllers are suitable for real-time implementations and have found their application in the nonlinear optimal integrated vehicle dynamic controllers.[20,21] These controllers are also used in optimal motion planning of unmanned ground vehicles.[22] Researchers have used the SDRE controllers for developing various active steering strategies such as lateral path tracking in limit handling conditions.[23–25] SDRE controller is popular in robotic control as well. Researchers have proved the SDRE controller to be effective in swinging up and stabilizing both single and double pendulum models in their respective equilibrium positions.[26,27] Consequently, the SDRE controller has found its application in the optimal control of underactuated single and double-link mobile robot platforms.[28,29] The SDRE controllers have never been used for recovering a vehicle model from the tip-over point.

The objective and organization of the study

This paper proposes a novel gain-scheduled SDRE anti-rollover controller designed using the IDPC vehicle model, that can reinstate a vehicle in an on-road and high-speed tip-over point. Figure 1 presents the complete logical flow diagram of the article.

The study begins with the design and analysis of the SDRE anti-rollover controller using the IDPC model with a virtual rollover torque instead of the real gravity torque. In the next stage, the proposed anti-rollover controller is evaluated with the IDPC model with the real gravity torque. The controller appeared to propose a high control input force towards the landing phase, where the vehicle is about to touchdown the ground. The next stage of the study proposes an effective method to keep the control input force within the saturation limits by relaxing the weight value corresponding to the roll angle of the vehicle (W_{θ_1}) based on the roll rate achieved by the model in the landing phase. Subsequently, the study proposes to use the SDRE anti-rollover controller, along with the relaxation for the landing phase, as a gain-scheduled lookup table in a two-dimensional (2D) space of θ_1 and $\dot{\theta}_1$. In
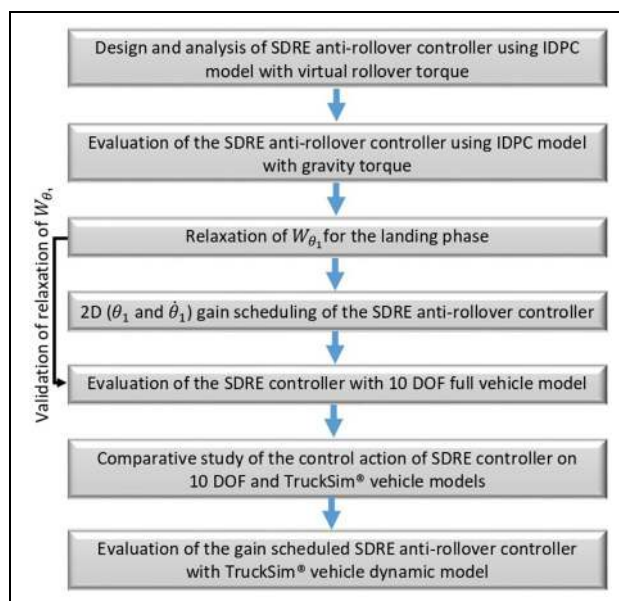

Figure 1. Organization of the contents.
SDRE: State-dependent Riccati equation; DOF: degrees of freedom.

the subsequent stage, the proposed gain-scheduled SDRE controller is evaluated with a 10-DOF full vehicle analytical model along with a nonlinear pure slip tyre model. The study incorporates a model that proposes the wheel steer angle corresponding to a lateral tyre input force proposed by the anti-rollover controller. The model is an inversion of the nonlinear pure slip tyre model. As shown in Figure 1, the validation of the assumptions made for determining the reduced value of W_{θ_1} for the landing phase in the third stage is also presented in this section. The final stage evaluates the gain-scheduled SDRE anti-rollover controller with the sophisticated TruckSim® vehicle dynamic model. Initially, the study presents a comparative study of the control action of the SDRE anti-rollover controller with the 10-DOF full vehicle model and the TruckSim® model. In the final stage of the study, the gain-scheduled anti-rollover controller is evaluated with the highly sophisticated TruckSim® vehicle dynamic software in various real-life initial conditions.

The IDPC vehicle model

The IDPC vehicle model can be used to predict the dynamics of a four-wheeled vehicle at a near tip-over point.[12] The analogy between the two above-mentioned models is exhibited in Figure 2. The IDPC vehicle model has two interconnected links of lengths l_1 and l_2 corresponding to unsprung and sprung masses of values m_1 and m_2, respectively. The torsional spring and damper correspond to the suspension dynamics of the vehicle. The massless cart corresponds to the tyre–road contact point. The axle angle offset is assumed as θ_0. The IDPC vehicle model has 3 DOF: roll motion of the vehicle (θ_1), relative roll motion of the sprung mass with respect to the vehicle (θ_2) and lateral motion of the vehicle (y).

Equation (1) describes the nonlinear dynamical equations of motion of the IDPC model with $\mathbf{q} = [y, \theta_1, \theta_2]^T$ and $\mathbf{B} = [1, 0, 0]^T$. f is the lateral traction force acting on the tyres

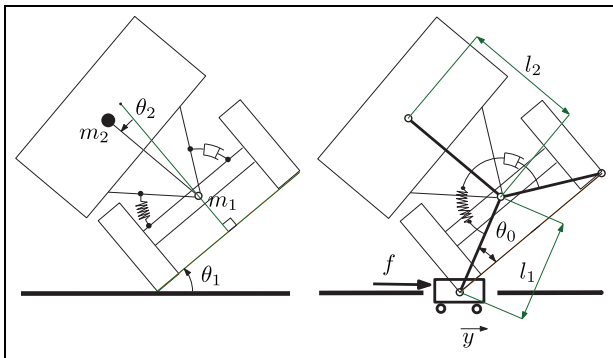$$\mathbf{H(q)}\ddot{\mathbf{q}} + \mathbf{C(q, \dot{q})}\dot{\mathbf{q}} + \mathbf{P(q)} = \mathbf{B}f \tag{1}$$

Figure 2. The IDPC model.
IDPC: inverted double pendulum on a massless cart.

where $\mathbf{H(q)}$ is the mass matrix, $\mathbf{C(q, \dot{q})}$ incorporates coriolis and centripetal components and $\mathbf{P(q)}$ represents spring potential as well as gravitational forces

$$\mathbf{H(q)} = \begin{bmatrix} m_1 + m_2 & h_{12} & h_{13} \\ h_{12} & h_{22} & h_{23} \\ h_{13} & h_{23} & m_2 l_2^2 + J_2 \end{bmatrix}$$

$$h_{12} = -l_1 sin(\theta_0 + \theta_1)(m_1 + m_2) - l_2 m_2 cos(\theta_1 + \theta_2)$$

$$h_{22} = (m_1 + m_2)l_1^2 + 2m_2 l_1 l_2 sin(\theta_0 - \theta_2) + m_2 l_2^2 + J_1 + J_2$$

$$h_{23} = m_2 l_2^2 + m_2 l_1 l_2 sin(\theta_0 - \theta_2) + J_2$$

$$h_{13} = -l_2 m_2 cos(\theta_1 + \theta_2)$$

$$\mathbf{C(q, \dot{q})} = \begin{bmatrix} 0 & c_1 & c_2 \\ 0 & 2_{c3}\theta_2 & c_3 \theta_2 \\ 0 & -c_3 \theta_1 & b_1 \end{bmatrix}$$

$$c_1 = c_2 - (m_1 + m_2)l_1 cos(\theta_0 + \theta_1)\dot{\theta}_1$$

$$c_2 = l_2 m_2 sin(\theta_1 + \theta_2)(\dot{\theta}_1 + \dot{\theta}_2)$$

$$c_3 = -m_2 l_1 l_2 cos(\theta_0 - \theta_2)$$

$$\mathbf{P(q)} = \begin{bmatrix} 0 \\ \tau_g \\ -m_2 g l_2 \sin(\theta_1 + \theta_2) + \tau \end{bmatrix}$$

$$\tau_g = (m_1 + m_2)g l_1 cos(\theta_0 + \theta_1) - m_2 g l_2 sin(\theta_1 + \theta_2)$$

$$\tau = k_1 \theta_2 + k_5 \theta_2^5$$

$$\tag{2}$$

The symbols τ_g and τ indicate the torque experienced by the IDPC vehicle model due to gravity and suspension spring, respectively.

In the present study, the vehicle is assumed to be moving only on the two wheels on one side with wheels on the other side lifted off the ground. This study proposes to recover the vehicle from this tip-over point by controlling the lateral force on the tyres which are on the ground. Any instances where these two wheels also lift-off from the ground, making the vehicle a projectile, are beyond this study's scope. The normal reaction force acting on the tyre and road contact point of the wheels, which are on the ground, is presented in equation (3). Hence, it must be noted that $F_n > 0$ always

$$\begin{aligned} F_n = {} & (m_1 + m_2)g + (m_1 + m_2)l_1 cos(\theta_0 + \theta_1)\ddot{\theta}_1 \\ & -m_2 l_2 sin(\theta_1 + \theta_2)(\ddot{\theta}_1 + \ddot{\theta}_2) \\ & -(m_1 + m_2)l_1 sin(\theta_0 + \theta_1)\dot{\theta}_1^2 \\ & -m_2 l_2 cos(\theta_1 + \theta_2)(\dot{\theta}_1 + \dot{\theta}_2)^2 \end{aligned} \tag{3}$$

For a coefficient of friction μ, the lateral tyre force (F_L) must be

$$-\mu F_n \leqslant F_L \leqslant \mu F_n \tag{4}$$

Table 1 displays the values of the various parameters of the IDPC vehicle model used for the study. The fifth-order stiffness corresponds to the nonlinear stiffness of the suspension system, which comes into play for large deflections. The specifications are of a standard Pick-up

Table 1. Specifications of the IDPC model.

Description	Symbol	Value
Unsprung mass	m_1	730 kg
Sprung mass	m_2	2000 kg
Roll MI-unsprung mass	J_1	250 kg m^2
Roll MI-sprung mass	J_2	750.5 kg m^2
Axle angle offset	θ_0	0.4 rad
Axle-link length	l_1	1 m
Sprung mass-link length	l_2	0.31 m
Linear stiffness	k_1	2.72×10^5 Nm/rad
Fifth-order stiffness	k_5	1.08×10^7 Nm/rad^5
Linear damping	b_1	1.69×10^4 Nm/(rad/s)

IDPC: inverted double pendulum on a massless cart; MI: moment of inertia.
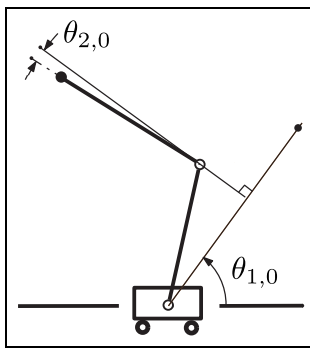
**Figure 3.** The unstable equilibrium point.

truck model present in the industrial standard TruckSim® vehicle dynamic simulation software.[30] A high centre of gravity (CG) vehicle model is chosen for the study as it is more susceptible to rollover than low CG vehicles.

Figure 3 shows the unstable equilibrium point of the IDPC model and the values of roll states $\theta_{1,0}$ and $\theta_{2,0}$ obtained are 0.9788 rad and 0.0188 rad, respectively. In this study, this limiting rollover point of the vehicle dynamics system is used as a reference point to ascertain the performance of the designed anti-rollover controller in the later sections. It was found in a simulation study that the IDPC vehicle model can closely follow the dynamics of a sophisticated full vehicle model when it is present in the region near this unstable equilibrium point $(\theta_{1,0}, \theta_{2,0})$.[18] Hence, the IDPC vehicle model is suitable for designing control systems to reinstate a vehicle from a tip-over scenario where the wheels on one side are in lifted-off condition.

Design of SDRE anti-rollover controller using the IDPC model with virtual rollover torque

IDPC model with virtual rollover torque

The DOF θ_1 measures the roll motion of the IDPC model, and τ_g indicates the gravitational torque acting
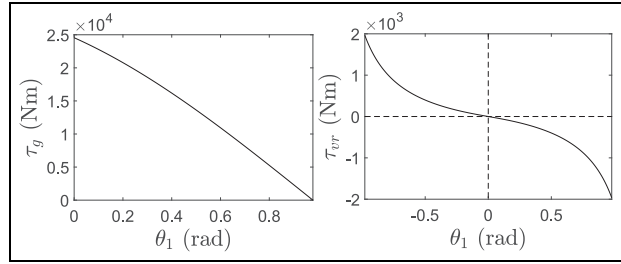
Figure 4. Gravitational and virtual torques.

on the model. Figure 4 shows the change in value of τ_g with respect to θ_1 for a constant value of $\theta_2 = \theta_{2,0}$. It is intuitive that in the range of $0 \leqslant \theta_1 < \theta_{1,0}$, gravitational torque aids the anti-rollover controller in reinstating a vehicle from the tip-over point. It can also be observed from the graph that starting from $\theta_1 = 0$, the value of τ_g decreases and becomes 0 at $\theta_1 = \theta_{1,0}$, which results in the establishment of the unstable equilibrium at the point $(\theta_{1,0}, \theta_{2,0})$. Hence, the assistance provided by the gravity torque at the tip-over region is minimal. This study aims to formulate an anti-rollover controller to reinstate a vehicle from the tip-over region using the SDRE method. The point $(\theta_{1,0}, \theta_{2,0})$ forms a singularity point for the SDRE method. In the design procedure of the anti-rollover controller, gravity torque is assumed to be zero in the entire range $0 \leqslant \theta_1 < \theta_{1,0}$ and a virtual rollover torque τ_{vr} is introduced.[31] Figure 4 also shows the nature of τ_{vr}, and it must be noted that the sense of τ_{vr} is the opposite of τ_g. It indicates the virtual torque's tendency to roll the vehicle over. It allows elimination of the singularity point $(\theta_{1,0}, \theta_{2,0})$ and creates a new virtual unstable equilibrium point on the ground at $(\theta_1, \theta_2) = (0, 0)$. The anti-rollover controller performs the recovery of the vehicle by attempting to bring the vehicle to the new virtual unstable equilibrium point on the ground at $(\theta_1, \theta_2) = (0, 0)$. In the conventional methods such as NMPC, a highly nonlinear piecewise function is used to emulate the ground dynamics to generate an equilibrium point on the ground. But this piecewise function made those controller formulations further complex.

The proposal in this study is to design a controller for a system that is highly susceptible to rollover and to use it for the original system, which is relatively more stable. This will result in a little overestimation of the control input force. The control input force will not be significantly high as the order of τ_{vr} is 10^3 compared to the order of 10^4 of the gravity torque. In the given scenario, an actuator is not available to directly generate the control input force, unlike in the standard control problems. The proposed input control force is generated on the tyres using a wheel steer angle actuator. It is justifiable to use an overestimate of the control input force due to the following reasons. First, attempting to generate a force on tyres that is a little over the saturation force for a brief duration will not adversely affect the steering system as it is prevalent during harsh

driving. Second, the accurate estimation of the normal reaction force available on the tyre–road contact point to determine the saturation conditions is challenging. At the same time, the wheel steer angle actuator needs to follow the saturation conditions strictly. The wheel steer angle model corresponding to the control input force used in this study incorporates a separate saturation condition to address this issue. It can be observed in the later sections that the wheel steer angles generated in these studies are in the nominal range.

Equation (5) represents the formulation of the proposed virtual rollover torque. The formulation is inspired by shape functions used in Pacejka tyre model[32]

$$\tau_{vr} = - V_d \tan\left(V_c \tan^{-1}(V_b \phi)\right) \tag{5}$$

where

$$\phi = (1 - V_e)\theta_1 V_f + \frac{V_e}{V_b} \tan^{-1}(V_b \theta_1 V_f)$$

The values of the shape determining coefficients V_b, V_c, V_d, V_e and V_f corresponding to the shape of τ_{vr} are 0.244, 1.1, 100, −0.132 and 20, respectively. This particular shape of τ_{vr} is chosen because it makes the system unstable in the range near $(\theta_{1,0}, \theta_{2,0})$ and readily drops to zero as the states approach $(0, 0)$. This results in the unstable equilibrium point of the virtual IDPC vehicle model at $(0, 0)$.

For the IDPC vehicle model with virtual rollover torque

$$\mathbf{P}^\star(\mathbf{q}) = \begin{bmatrix} 0 \\ \tau_{vr} \\ \tau \end{bmatrix} \tag{6}$$

where $\mathbf{P}^\star(\mathbf{q})$ contains the virtual rollover torque and spring potential forces. The nonlinear dynamical equation of motion of the system becomes

$$\mathbf{H}(\mathbf{q})\ddot{\mathbf{q}} + \mathbf{C}(\mathbf{q}, \dot{\mathbf{q}})\dot{\mathbf{q}} + \mathbf{P}^\star(\mathbf{q}) = \mathbf{B}f \tag{7}$$

Design of SDRE anti-rollover controller

SDRE method is an extended nonlinear version of the LQR method, which accounts for the nonlinearities involved in the problem, yet is simple in terms of the computation time. It provides an approximate nonlinear solution to a nonlinear performance index minimization problem subject to a system equation.[26,33] There are numerous ways of representing a nonlinear dynamical system in the state-dependent coefficient (SDC) form. All such formulations may not be a stabilizable parameterization of the nonlinear system.[33] The choice of the coefficient matrices presented in equation (7) forms a valid combination in a stabilizable parameterization of the nonlinear IDPC vehicle model.

The nonlinear system in pseudo-linear SDC form with $\mathbf{X} = (\mathbf{q}, \dot{\mathbf{q}})$ is

$$\mathbf{X} = \overline{\mathbf{A}}(\mathbf{X})\mathbf{X} + \overline{\mathbf{B}}(\mathbf{X})f \tag{8}$$

The output equation is

$$\mathbf{q} = \mathbf{D}\mathbf{X} + \mathbf{E}f \tag{9}$$

The SDC matrix $\overline{\mathbf{A}}(\mathbf{q}, \mathbf{q})$ is

$$\overline{\mathbf{A}}(\mathbf{q}, \dot{\mathbf{q}}) = \begin{bmatrix} 0 & \mathbf{I} \\ -\mathbf{H}^{-1}\mathbf{G} & -\mathbf{H}^{-1}\mathbf{C} \end{bmatrix} \tag{10}$$

where

$$\mathbf{G}(\mathbf{q}) = \begin{bmatrix} 0 & 0 & 0 \\ 0 & \dfrac{\tau_{vr}}{\theta_1} & 0 \\ 0 & 0 & \dfrac{\tau}{\theta_2} \end{bmatrix} \tag{11}$$

The SDC matrix $\overline{\mathbf{B}}(\mathbf{q})$ is

$$\overline{\mathbf{B}}(\mathbf{q}) = \begin{bmatrix} \mathbf{0} \\ -\mathbf{H}^{-1}\mathbf{B} \end{bmatrix} \tag{12}$$

The coefficient matrices in the output equation (9) are $\mathbf{D} = [\mathbf{I}\,\mathbf{0}_{3\times3}]$, where $\mathbf{I}$ is the identity matrix and $\mathbf{E} = 0$. The performance criterion J of the SDRE optimal control problem is

$$J = \frac{1}{2}\int_0^\infty (\mathbf{X}^T\mathbf{Q}\mathbf{X} + f^T Rf)\,dt \tag{13}$$

where $\mathbf{Q} = \overline{\mathbf{D}}^T\overline{\mathbf{D}}$ where

$$\overline{\mathbf{D}} = [\mathbf{D}^\star\,\mathbf{0}_{3\times3}] \quad \text{where} \quad \mathbf{D}^\star = \begin{bmatrix} 1 & 0 & 0 \\ 0 & W_{\theta_1} & 0 \\ 0 & 0 & 1 \end{bmatrix} \tag{14}$$

The reference value of relative weight for control effort f is assumed as $R = 1$. The control force corresponding to a particular set of states can be found as

$$f = - R^{-1}\overline{\mathbf{B}}^T(\mathbf{X})\mathbf{S}(\mathbf{X})\mathbf{X} \tag{15}$$

Hence, the gain matrix is $\mathbf{K}(\mathbf{X}) = R^{-1}\overline{\mathbf{B}}^T(\mathbf{X})\mathbf{S}(\mathbf{X})$ where the matrix $\mathbf{S}(\mathbf{X})$ can be obtained as the steady state solution of the differential Riccati equation shown below

$$\mathbf{S}(\mathbf{X})\overline{\mathbf{A}}(\mathbf{X}) + \overline{A}^T(\mathbf{X})\mathbf{S}(\mathbf{X})$$
$$-\mathbf{S}(\mathbf{X})\overline{\mathbf{B}}(\mathbf{X})\mathbf{R}^{-1}\overline{\mathbf{B}}^T(\mathbf{X})\mathbf{S}(\mathbf{X}) + \mathbf{Q}(\mathbf{X}) = 0 \tag{16}$$

Evaluation of SDRE controller with IDPC model with virtual rollover torque

It was stated that the SDRE-based anti-rollover controller performs the recovery action of the vehicle in a tip-over scenario by attempting to bring and settle the vehicle to the unstable equilibrium point at $(0, 0)$ on the ground. The control action of the anti-rollover controller designed with the SDRE method is evaluated with
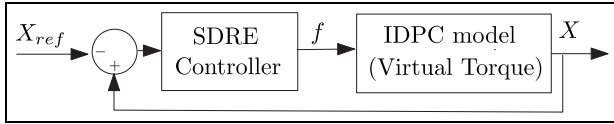
Figure 5. Application of SDRE controller to IDPC model with virtual rollover torque.
SDRE: State-dependent Riccati equation; IDPC: inverted double pendulum on a massless cart.
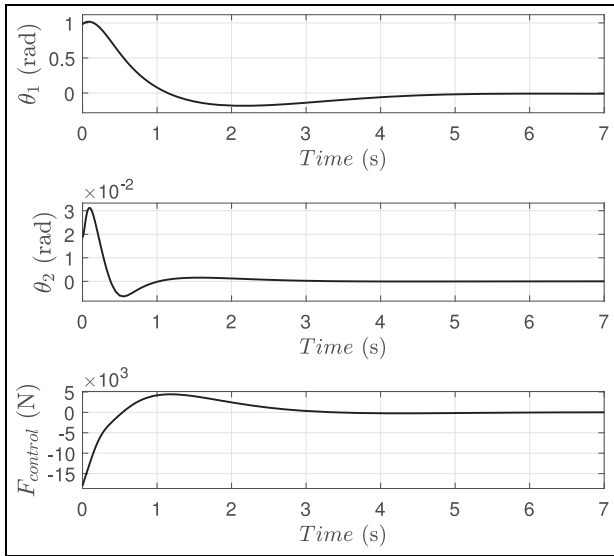

Figure 6. Settlement of IDPC model with virtual rollover torque to the equilibrium point on the ground.
IDPC: inverted double pendulum on a massless cart.

Figure 7. Change in value of SDRE gains with time.
SDRE: State-dependent Riccati equation.

the IDPC model with virtual rollover torque presented in equation (7) by implementing it in MATLAB®/ Simulink®. Figure 5 shows the layout in which the SDRE-based anti-rollover controller is applied to the IDPC model with virtual rollover torque. X_{ref} denotes the reference unstable equilibrium point on the ground.

Figure 6 shows the control action performed by the SDRE-based anti-rollover controller. For the simulation, the initial conditions chosen are $\theta_1 = \theta_{1,0}$, $\theta_2 = \theta_{2,0}$, $\dot{\theta}_1 = 1.2$ rad/s and $\dot{\theta}_2 = 0$ rad/s. The initial conditions indicate that the vehicle is assumed to start at the unstable equilibrium point. A positive initial roll rate of 1.2 rad/s emulates an extremely severe impending rollover situation that may occur in a practical condition.

The W_{θ_1} value, which is a measure of the weight of roll state θ_1 in the matrix $\overline{\mathbf{D}}$, is taken as 10^4 for this simulation. Values of W_{θ_1} of order 4 can generate control input force values in a range that is sufficient, as well as achievable in a practical vehicle rollover scenario. The subsequent sections discuss the effect of change in the value of W_{θ_1} in the control action of the anti-rollover controller. During the simulation, as shown in Figure 6, the controller recovers the vehicle model from the tip-over point and settles it in the
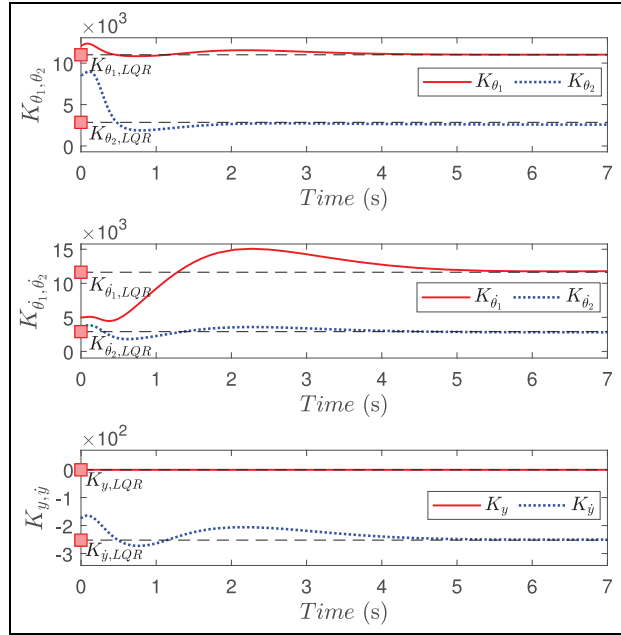
unstable equilibrium point on the ground. The figure also shows the control force applied to the model with time. The change in the value of SDRE gains corresponding to each state variable of the IDPC model with virtual rollover torque as a function of time is presented in Figure 7. The graphs also show the constant gain values obtained in the LQR method by linearizing the model at the unstable equilibrium point $(0, 0)$ on the ground.

Unlike the graphs that contrast the LQR method, SDRE gains are dependent on the state of the system and vary with time. The SDRE gains K_{θ_1} and K_{θ_2} corresponding to θ_1 and θ_2, respectively, assume higher values at the near rollover point. It can also be noted that as the system settles to the unstable equilibrium point, the SDRE gain values tend to merge with the constant LQR gain values. It is evident that the proposed anti-rollover controller can recover the vehicle model from the tip-over point and stabilize the IDPC model with virtual rollover torque to the unstable equilibrium point on the ground at $(\theta_1, \theta_2) = (0, 0)$.

Evaluation of SDRE controller with IDPC model with gravity torque

The previous section illustrated the design and evaluation of the anti-rollover controller with the IDPC model with virtual rollover torque. It must be noted that the IDPC vehicle model with virtual rollover torque was utilized only for the formulation of the SDRE controller, and the performance of the anti-rollover controller with the real-life IDPC vehicle model with gravity torque is of significance. Besides, in a real-life scenario, the moment θ_1 becomes zero foremost, the
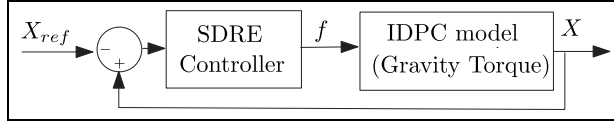
Figure 8. Application of SDRE controller to IDPC model with gravity torque.
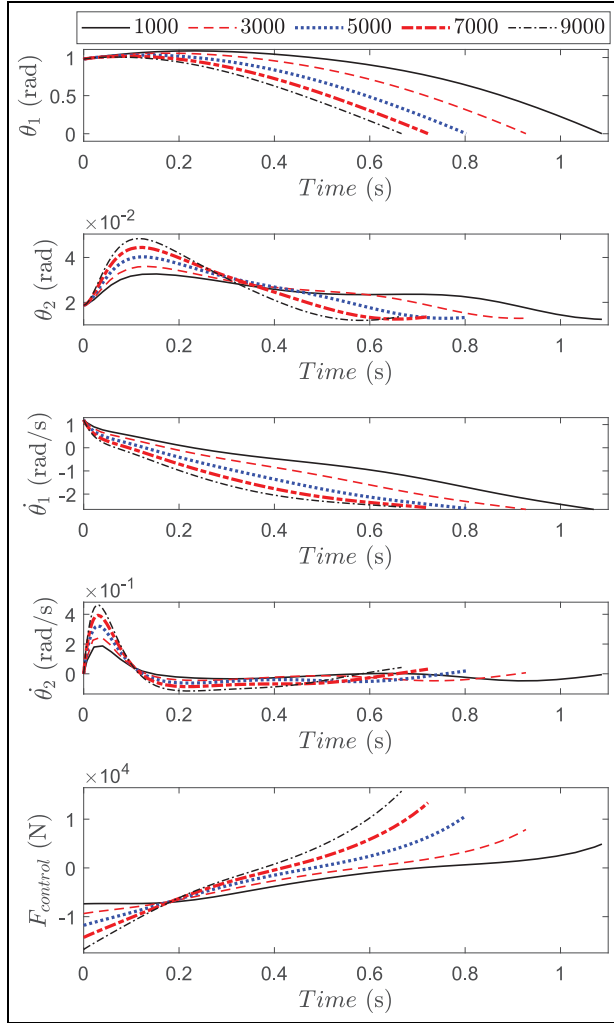SDRE: State-dependent Riccati equation; IDPC: inverted double pendulum on a massless cart.

Figure 9. Effect of change in W_{θ_1} in control action.

vehicle changes from the two-wheeled to four-wheeled model as the ground dynamics come into the picture. A negative value of θ_1 has no physical meaning. In Figure 6, the simulation was extended until 7 s to assess the stability of the closed loop system and the time only until 1.156 s where the value of θ_1 becomes zero foremost is of interest in further studies. This section analyzes the performance of the anti-rollover controller in conjunction with the IDPC model with gravity torque by implementing the system in MATLAB®/Simulink®. Figure 8 exhibits the layout in which the SDRE controller is applied to the IDPC model with gravity torque. Besides, a study on change in control action of the anti-rollover controller with variation in the weight,

W_{θ_1}, is done. Figure 9 presents the results obtained from the simulation study. All the simulations were started from the same initial conditions $\theta_1 = \theta_{1,0}$, $\theta_2 = \theta_{2,0}$, $\dot{\theta}_1 = 1.2$ rad/s as mentioned in the previous section.

The value of the weight W_{θ_1} was varied from 1×10^3 to 9×10^3. From Figure 9, it is evident that the control input force generated increased with an increase in the value of W_{θ_1}. This increase in the control force resulted in a decrease in the time over which the IDPC model was recovered to ground. This shows the suitability of the weight value W_{θ_1} as the performance tuning parameter of the SDRE controller.

Relaxation of W_{θ_1} for the landing phase

The previous section depicted the impact of change in the value of W_{θ_1} in the control action of the SDRE anti-rollover controller through multiple simulations with different W_{θ_1} values. However, it must be noted that in each simulation, the value of W_{θ_1} was kept constant throughout. The trend followed by the control input force is shown in Figure 9 towards the landing phase, where θ_1 is close to 0 and $\dot{\theta}_1 < 0$ draws attention. In the landing phase, the SDRE controller tends to suggest an input force, which is even higher than the values observed during the recovery phase, where the initial conditions were close to the tip-over point. Theoretically, the SDRE controller is attempting to stabilize the IDPC model at the pseudo unstable equilibrium point on the ground at $(0, 0)$. But in the real model, gravity torque exists instead of virtual rollover torque. Due to this dominant action of the gravity torque in the landing phase, the IDPC model achieves a high roll rate close to -2.5 rad/s towards the end of the simulation. The control force's high values are proposed to settle the vehicle model that approaches the equilibrium point with such a high roll rate. However, in a real-life scenario, as the vehicle approaches the landing phase, the normal reaction tyre forces tend to drop down readily, resulting in low values of saturation force according to equation (4). Hence, such high values of lateral tyre forces proposed by the anti-rollover controller are not achievable in the landing phase.

This section proposes an approximate method for choosing the values of W_{θ_1} for the landing phase with respect to the roll rate of the model $\dot{\theta}_1$ so that the proposed control force stays within the saturation limit. Equation (3) presented the normal reaction force F_n acting on the tyre–road contact point of the IDPC vehicle model. The first subplot of Figure 10 presents the variation of lateral saturation tyre force μF_n with the value of $\dot{\theta}_1$ obtained using equation (3) at the landing phase. In the plot, the roll angles θ_1 and θ_2 are taken as 0, since the vehicle is in the landing phase.

Figure 9 shows that, as the vehicle approaches landing time, the values of $\dot{\theta}_2$ and $\ddot{\theta}_2$ approaches 0. The figure also illustrates that the slope of $\dot{\theta}_1$ remains almost
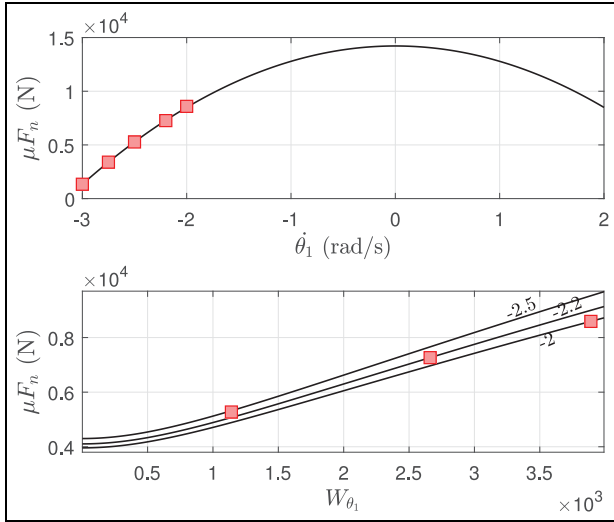
Figure 10. Saturation tyre force (μF_n) versus $\dot{\theta}_1$ and W_{θ_1}.

constant in the landing phase. Hence, an approximate average value of $\ddot{\theta}_1 = 4$ rad/s^2 is used for obtaining the plot. The markers in the first subplot of Figure 10 denote the saturation values, μF_n, at points $\dot{\theta}_1 = -2, -2.2, -2.5, -2.75$ and -3 rad/s. The second subplot of the same figure shows the saturation force μF_n against weight value W_{θ_1}. The graphs are plotted for roll rates $\dot{\theta}_1 = -2, -2.2$ and -2.5 rad/s. The marker on each plot here shows the value of W_{θ_1} corresponding to μF_n for that particular value of $\dot{\theta}_1$. It is evident from the second subplot that reducing the value of W_{θ_1} below a range makes the plots converge to a constant value. Hence, weight values corresponding to $\dot{\theta}_1 = -2.75$ and -3 rad/s are found to be out of bound, since the use of a lower weight does not help in obtaining a lower control force. Hence, a constant value of 1000 is used as the weight value for $\dot{\theta}_1 = -2.75$ and -3 rad/s. The final approximation of weight values obtained corresponding to $\dot{\theta}_1 = -2,$ $-2.2, -2.5, -2.75$ and -3 rad/s are 3891, 2661, 1141, 1000 and 1000, respectively. Figure 11 shows the incorporation of weight values obtained for the landing phase with the constant weight value used for the recovery phase. The value of W_{θ_1} starts its drop only from a value of $\dot{\theta}_1 = -1$ rad/s. In practical cases, such low values of roll rates below -1 rad/s occur only in the landing phase. It eliminates the possibility of this method, suggesting a low weight value when the vehicle is at a near tip-over point. The spline interpolation method is used to obtain the intermediate values to maintain a smooth transition of the weight value during the control action.

A simulation was conducted with the IDPC vehicle model with gravity torque using the SDRE controller with the relaxation of weight for the landing phase to understand the change occurring to the force proposed by the controller. Figure 12 presents the effect of the use of the variable W_{θ_1}. In the simulation, the IDPC model with gravity was reinstated from the initial
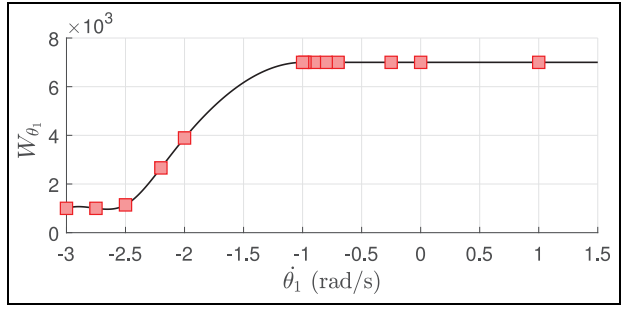

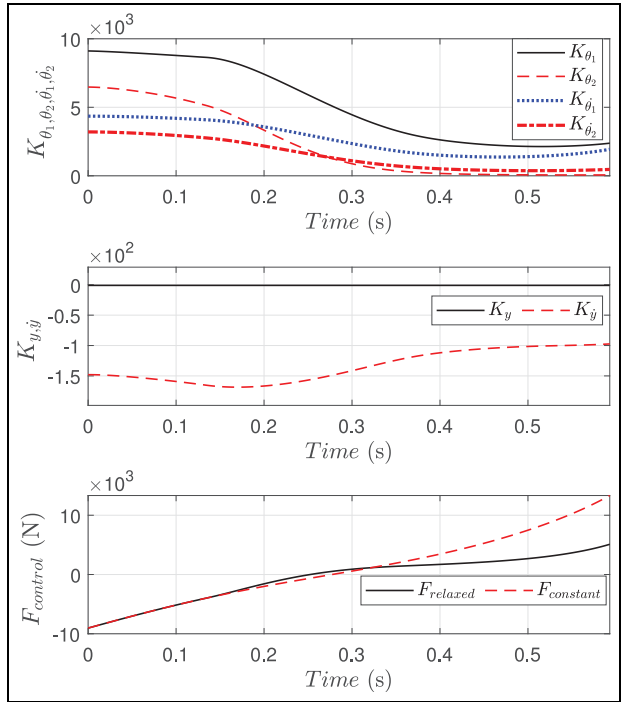**Figure 11.** Relaxation of W_{θ_1} for landing phase.

Figure 12. Change in control input force in landing phase due to relaxation of W_{θ_1}.

conditions $\theta_1 = \theta_{1,0}, \quad \theta_2 = \theta_{2,0}$ and $\dot{\theta}_1 = 1.2$ rad/s using the variable weight model presented in Figure 11. The first and second subplots of the figure show the reduction that occurred to the SDRE gain values corresponding to states of the IDPC vehicle model as the simulation proceeded to the landing phase. The third subplot depicts the subsequent reduction in the control input force as a result of the change in the weight value in the landing phase. The validation of the assumptions mentioned above can be found in Figure 21 in the subsection 'Validation of relaxation of W_{θ_1} for landing phase' under the section 'Evaluation of the SDRE controller with 10-DOF full vehicle model'.

The 2D (θ_1 and $\dot{\theta}_1$) gain-scheduling of the SDRE controller

The previous sections presented the SDRE controller design using the IDPC model with virtual rollover torque, with a relaxation of the weight W_{θ_1} for the landing
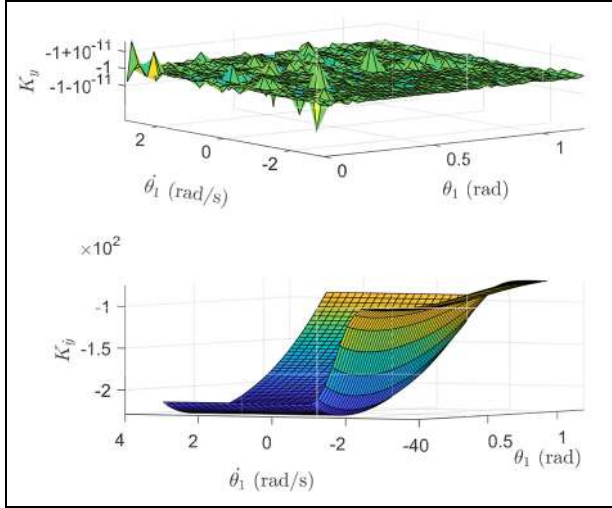
Figure 13. The 2D gain-scheduled K_y and $K_{\dot{y}}$.
2D: two-dimensional.

phase. The SDRE controller needs to solve the non-linear performance index minimization problem in real-time for every sampling time in the current form. It is essential to note the dependencies of the state variables on the determined values of the SDRE gains. The coefficient matrices $\overline{\mathbf{A}}(\mathbf{X})$ and $\overline{\mathbf{B}}(\mathbf{X})$ in equation (8) do not contain y and $\dot{y}$. So the state feedbacks of lateral displacements do not affect the determination of the SDRE gains. From Figure 12, it can be pointed out that the gain values K_y and $K_{\dot{y}}$ corresponding to y and $\dot{y}$, respectively, are relatively constant for change in states compared to the other gain values. Besides, the order of gains corresponding to lateral displacement is 10^2 compared to an order of 10^3 of the other SDRE gains. In addition, the state variables θ_2 and $\dot{\theta}_2$ have relatively small orders of 10^{-2} and 10^{-1}, respectively. These observations lead to the conclusion that θ_1 and $\dot{\theta}_1$ are the only two state variables that have a dominant effect on computing SDRE gains. Figures 13 and 14 present all the gain values in θ_1 and $\dot{\theta}_1$ planes for constant values of $\theta_2 = \theta_{2,0}$ and $\dot{\theta}_2 = 0$.

Henceforth, the SDRE gain values can be used as a 2D gain-scheduled controller by presenting the gain values just as a lookup table of these graphs rather than solving the nonlinear optimal problem in every step. For a controller to perform well in real-time, the computational time required must be less than the sampling time. This criterion is highly relevant in the current problem where the vehicle is near the tip-over point, and the response time available is minimal. The computation time taken in MATLAB® for the gain-scheduled SDRE controller is of the order of 10^{-2}, whereas a nonlinear optimal controller (NMPC) takes 0.4 s per sample for the recovery of IDPC vehicle model from tip-over point.[14] The computation time can be made negligibly small by using better search algorithms. For instance, the variation of θ_1 and $\dot{\theta}_1$ in the given dynamic system will always be continuous, and any future
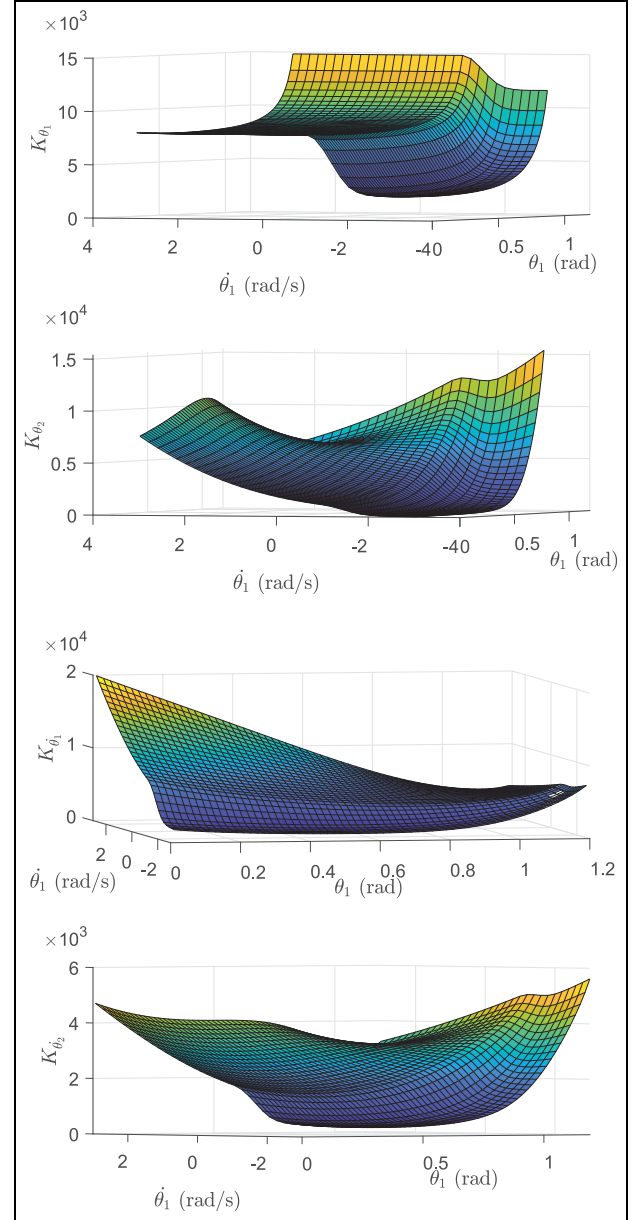

Figure 14. The 2D gain-scheduled K_{θ_1}, K_{θ_2}, $K_{\dot{\theta}_1}$ and $K_{\dot{\theta}_2}$.
2D: two-dimensional.

update will always lie in the vicinity of current states. It is not needed to restart the search algorithm all over again every time. Direct implementation in a C++ platform will further reduce the computation time. The energy-based controller is the simplest form of the nonlinear controller, and the negligible computation time makes it an ideal controller for real-time implementations.[18] But the energy-based controller is not optimal and has no direct control over the control input force generated. The control input force is generated based on the inherent nonlinear nature of the controller. The nonlinear nature becomes aggressive, especially in highly severe scenarios, and tends to propose control input forces beyond the limits of saturation condition.

It is essential to validate all the assumptions mentioned above. A comparative study is conducted using simulations where the IDPC vehicle model was
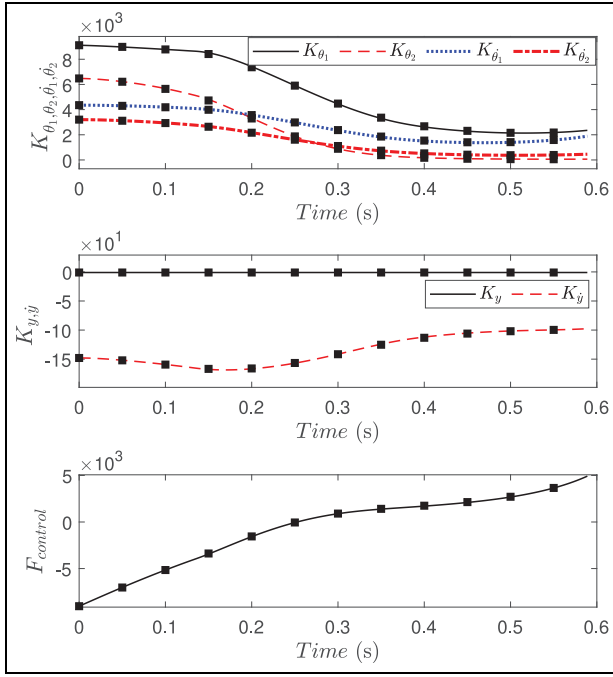
Figure 15. Comparison of gain-scheduled and direct optimal solution SDRE controllers.
SDRE: State-dependent Riccati equation.

Figure 16. Schematic diagram of 10-DOF model.
DOF: degrees of freedom.

recovered from the initial conditions $\theta_1 = \theta_{1,0}$, $\theta_2 = \theta_{2,0}$ and $\dot{\theta}_1 = 1.2$ rad/s using the SDRE controller with and without gain-scheduling.

Figure 15 shows the values of the SDRE gains and the final control input force generated during the simulations. In the graphs, solid lines correspond to the SDRE controller without gain-scheduling. The symbol ■ indicates the corresponding gain values and the control input force at the same time from a gain-scheduled SDRE controller. It is evident from the graphs that the two cases are indistinguishable, and it validates all the assumptions stated before on the state dependencies.

The 10-DOF full vehicle model

A simple model, such as an IDPC vehicle model that captures only the dominant dynamic effects, is preferred for controller design to keep the controller's complexity at a minimum. It must be investigated if the controller can perform satisfactorily in the presence of all the dynamic effects that were not considered in the formulation of the anti-rollover controller. This section presents a 10-DOF full vehicle model, along with a nonlinear pure slip tyre model, which is used to evaluate the performance of the SDRE controller in the following sections.

The 10-DOF model

Figure 16 presents the configuration of the 10-DOF full vehicle model. The vehicle is assumed to have front and rear axle suspension systems. The model has one sprung
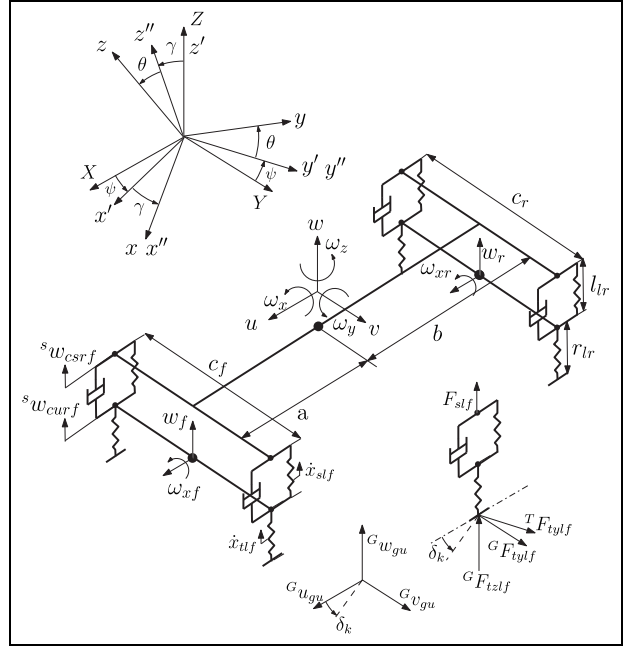
mass and two unsprung masses. The unsprung masses correspond to the front and rear axles.

The inertia, stiffness and damping properties of the model are assumed the same as the TruckSim® vehicle dynamics model to maintain the overall generality of the study. The sprung mass has three translational (u, v and w) and three rotational (ω_x, ω_y and ω_z) motions in the Cartesian directions X, Y and Z. Each of the unsprung masses has vertical translational (w_f and w_r) and rotational (ω_{xf} and ω_{xr}) motions. The roll, pitch and yaw angles of the vehicle are denoted by θ, γ and ψ, sequentially. The superscripts s, G and T denote sprung mass, ground and tyre coordinate systems, respectively; w_{cs} and w_{cu} denote vertical velocities at the corners of sprung and unsprung masses, respectively. The tyre and suspension deflection are denoted by x_s and x_t, respectively. Suspension and tyre forces are denoted by F_s and F_t. In general, the subscript ij is used such that i can be l or r for left and right, respectively, and j can be f and r for front and rear, respectively. δ_k denotes the steer angle about the kingpin axis. Figure 17 shows the configuration in which the 10-DOF full vehicle model with a nonlinear pure slip tyre model is implemented in MATLAB®/Simulink® environment. The inputs and outputs of each block are denoted in the diagram.

The steer angle (δ_k) is the input (I/P) to the model. All the state variables of the model constitute the output 1 (O/P-1). The normal reaction tyre forces, ground velocities and slip angles of the tyres on the ground constitute output 2 (O/P-2). The model is organized as blocks. The mathematical formulations used in each block are described below. The table containing the
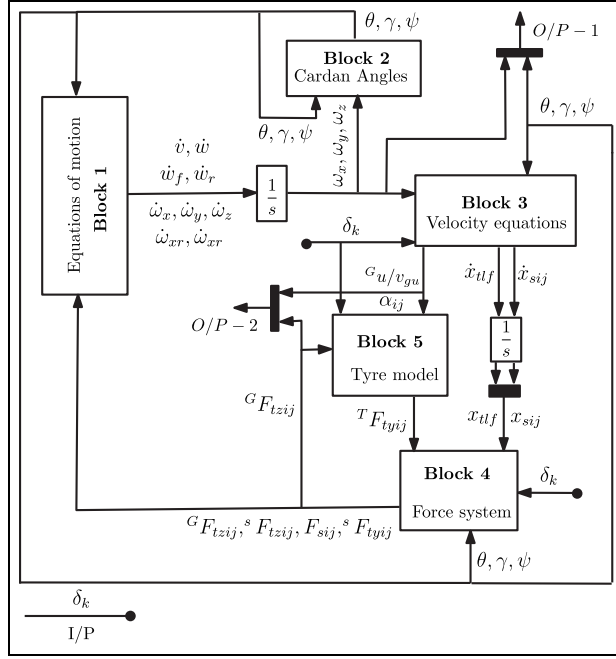
Figure 17. Block diagram of Simulink® implementation of the 10-DOF model.
DOF: degrees of freedom.

specifications and notations of the 10-DOF full vehicle model can be found in Appendices 1 and 2.

Block 1: The equations of motion of the 10-DOF system are incorporated in this block. The vehicle model is assumed to have 10 DOF. The controller's recovery action happens in a short span of time, and within that, it is reasonable to assume the longitudinal velocity u to be a constant. The equations of motion of heave (w) and lateral (v) motion of the sprung mass are as follows

$$m_t\dot{v} = \sum {}^sF_{tyij} - m_t g\sin(\theta)\cos(\gamma) - m_t(\omega_z u - \omega_x w)$$
$$m\dot{w} = \sum F_{sij} - mg\cos(\theta)\cos(\gamma) - m(\omega_x v - \omega_y u) \quad (17)$$

The equations of roll (ω_x), pitch (ω_y) and yaw (ω_z) motions of the sprung mass are as follows

$$J_x\dot{\omega}_x =$$
$$\sum\left[{}^sF_{tyij}l_{ij} - \frac{1}{2}\left(m_j g\sin(\theta)\cos(\gamma)\left(l_{lj} + l_{rj}\right) - m_j\left(l_{lj} + l_{rj}\right)\dot{v}\right)\right]$$
$$+ \frac{1}{2}\left(\left(F_{slf} - F_{srf}\right)c_f + \left(F_{slr} - F_{srr}\right)c_r\right)$$

$$J_y\dot{\omega}_y = \frac{1}{2}\sum\left[-m_j g\cos(\theta)\left(l_{lj} + l_{lj}\right) + m_j\left(l_{lj} + l_{lj}\right)\dot{v}\right]$$
$$+ \left(F_{slr} + F_{srr}\right)b - \left(F_{slf} + F_{srf}\right)a$$
$$J_z\dot{\omega}_z = {}^sF_{tylf}a - {}^sF_{tylr}b$$

$$\quad (18)$$

The equations of motion corresponding to heave motions of the front (w_f) and rear (w_r) axles are

$$m_f\dot{w}_f = {}^sF_{tzlf} - \left(F_{slf} + F_{srf}\right) - m_f g\cos(\theta)\cos(\gamma)$$
$$- m_f\left(\omega_{xf}v_f - \omega_y u_f\right)$$
$$m_r\dot{w}_r = {}^sF_{tzlr} - \left(F_{slr} + F_{srr}\right) - m_r g\cos(\theta)\cos(\gamma) \quad (19)$$
$$- m_r\left(\omega_{xr}v_r - \omega_y u_r\right)$$

Equations of motion corresponding to roll motions of the front (ω_{xf}) and rear (ω_{xr}) axles are

$$J_{xf}\dot{\omega}_{xf} = {}^sF_{tylf}r_{lf} + \frac{\left(-F_{slf} + F_{srf} + {}^sF_{tzlf}\right)c_f}{2}$$
$$J_{xr}\dot{\omega}_{xr} = {}^sF_{tylr}r_{lr} + \frac{\left(-F_{slr} + F_{srr} + {}^sF_{tzlr}\right)c_r}{2} \quad (20)$$

Block 2: The formulations for roll (θ), pitch (γ) and yaw (ψ) angles of the vehicle model are presented in this block

$$\dot{\theta} = \omega_x + \omega_y\sin(\theta)\tan(\gamma) + \omega_z\cos(\theta)\tan(\gamma)$$
$$\dot{\gamma} = \omega_y\cos(\theta) - \omega_z\sin(\theta)$$
$$\dot{\psi} = \omega_y\frac{\sin(\theta)}{\cos(\gamma)} + \omega_z\frac{\cos(\theta)}{\cos(\gamma)} \quad (21)$$

Block 3: The knowledge of all the state variables helps find the velocities at all the relevant points on the model. The formulations for the velocities are incorporated into this block. Velocities at the corners of the sprung mass are as follows

$$^sw_{cslf} = w + \frac{c_f\omega_x}{2} - a\omega_y$$
$$^sw_{cslr} = w + \frac{c_r\omega_x}{2} + b\omega_y$$
$$^sw_{csrf} = w - \frac{c_f\omega_x}{2} - a\omega_y \quad (22)$$
$$^sw_{csrr} = w - \frac{c_r\omega_x}{2} + b\omega_y$$

Velocities at the CG of the unsprung masses are

$$v_f = u - \frac{1}{2}\left(l_{lf} + l_{rf}\right)\omega_y$$
$$u_f = v + \frac{1}{2}\left(l_{lf} + l_{rf}\right)\omega_x + a\omega_z$$
$$v_r = u - \frac{1}{2}\left(l_{lr} + l_{rr}\right)\omega_y \quad (23)$$
$$u_r = v + \frac{1}{2}\left(l_{lr} + l_{rr}\right)\omega_x - b\omega_z$$

Velocities at the corners of the unsprung masses are

$$^{s}u_{culf} = u - \frac{(l_{lf} + l_{rf})\omega_y + c_f\omega_z}{2}$$

$$^{s}v_{culf} = v + \frac{(l_{lf} + l_{rf})\omega_x}{2} + a\omega_z$$

$$^{s}w_{culf} = w_f + \frac{c_f\omega_{xf}}{2}$$

$$^{s}u_{culr} = u - \frac{(l_{lr} + l_{rr})\omega_y + c_r\omega_z}{2}$$

$$^{s}v_{culr} = v + \frac{(l_{lf} + l_{rf})\omega_x}{2} + b\omega_z$$

$$^{s}w_{culr} = w_f + \frac{c_r\omega_{xr}}{2}$$

$$^{s}u_{curf} = u - \frac{(l_{lf} + l_{rf})\omega_y - c_f\omega_z}{2} \tag{24}$$

$$^{s}v_{curf} = v + \frac{(l_{lf} + l_{rf})\omega_x}{2} + a\omega_z$$

$$^{s}w_{curf} = w_f - \frac{c_f\omega_{xf}}{2}$$

$$^{s}u_{curr} = u - \frac{(l_{lr} + l_{rr})\omega_y + c_f\omega_z}{2}$$

$$^{s}v_{curr} = v + \frac{(l_{lr} + l_{rr})\omega_x}{2} + b\omega_z$$

$$^{s}w_{curr} = w_r - \frac{c_r\omega_{xr}}{2}$$

Now the deflection of suspensions attached to wheels which are on the ground can be written as

$$\dot{x}_{sij} = -^{s}w_{csij} + ^{s}w_{cuij} \tag{25}$$

The rate of tyre deflection can be taken as the velocity at the respective corner of the unsprung mass in ground coordinate system

$$^{G}w_{culj} = cos(\gamma)\left(^{s}w_{culj}cos(\theta) + ^{s}v_{culj}sin(\theta)\right)$$
$$\quad\quad\quad - ^{s}u_{culj}sin(\gamma)$$
$$\dot{x}_{tlj} = ^{G}w_{culj} \tag{26}$$

Slip angles of the wheels which are on the ground can be determined using the longitudinal and lateral velocities on the ground in ground coordinate system. Here θ_j can be roll angle of front axle (θ_f) or roll angle of rear axle (θ_r)

$$^{G}u_{gulj} = \left(^{s}u_{culj} - r_{lj}\omega_y\right)cos(\gamma)$$
$$\quad + \left(^{s}w_{culj}cos(\theta_j) + \left(^{s}v_{culj} + r_{lj}\omega_{xf}\right)sin(\theta_{1f})\right)sin(\gamma)$$

$$^{G}v_{gulj} = \left(^{s}v_{culj} + r_{lj}\omega_{xf}\right)cos(\theta_j) - ^{s}w_{clj}sin(\theta_j)$$

$$\tag{27}$$

From equation (27), slip angles can be obtained as

$$\alpha_{lf} = tan^{-1}\left(\frac{^{G}v_{gulf}}{^{G}u_{gulf}}\right) - \delta_k$$

$$\alpha_{lr} = tan^{-1}\left(\frac{^{G}v_{gulr}}{^{G}u_{gulr}}\right) \tag{28}$$

Block 4: The formulations corresponding to the system of forces acting on the model are presented in this block.

The suspension force can be written as

$$F_{sij} = k_{sij}x_{sij} + b_{sij}\dot{x}_{sij} \tag{29}$$

Normal reaction tyre force in ground coordinate system is

$$^{G}F_{tzlj} = k_{tlj}x_{tlj} \tag{30}$$

Lateral tyre force in ground coordinate system is

$$^{G}F_{tylf} = ^{T}F_{tylf}cos(\delta_k)$$
$$^{G}F_{tylr} = ^{T}F_{tylr} \tag{31}$$

Now the normal and lateral tyre forces in sprung mass coordinate system can be obtained as

$$^{s}F_{tzlj} = ^{G}F_{tzlj}cos(\theta)cos(\gamma) + ^{G}F_{tylj}cos(\delta_k)sin(\theta)$$
$$^{s}F_{tylj} = ^{G}F_{tylj}cos(\theta) - ^{G}F_{tzlj}cos(\gamma)sin(\theta) \tag{32}$$

Instantaneous tyre radius and suspension length can be written as

$$r_{ij} = \frac{r_0 - x_{tij}}{cos(\gamma)cos(\theta)}$$
$$l_{ij} = l_0 + x_{sij} \tag{33}$$

Tyre model

Block 5 in Figure 17 presents the nonlinear pure slip tyre model used, along with the 10-DOF full vehicle model. These data points as well are obtained from the tyre model used along with the previously mentioned pick-up truck model available in TruckSim® software. The curves are generated for a constant coefficient of friction $\mu = 0.85$, using the spline interpolation and extrapolation method. Figure 18 presents the one-sided tyre model for different normal reaction forces acting on the tyre.

Evaluation of the SDRE controller with 10-DOF full vehicle model

The current section evaluates the proposed gain-scheduled SDRE anti-rollover controller with the 10-DOF full vehicle model formulated in the previous section. Figure 19 exhibits the layout in which the SDRE
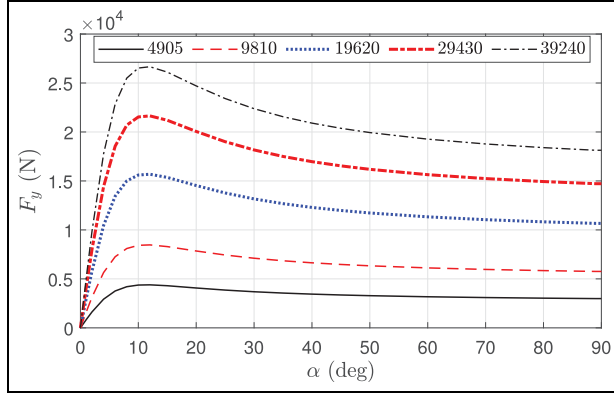
Figure 18. Characteristic curves of nonlinear tyre model.

Figure 19. SDRE controller applied to 10-DOF full vehicle model.
SDRE: State-dependent Riccati equation; DOF: degrees of freedom.

Figure 20. Characteristic curves of slip angle.

controller is applied to the 10-DOF model. The input (I/P) and the outputs (O/P-1 and O/P-2) mentioned here are the same as described in Figure 17. The gain-scheduled SDRE controller receives state feedback from the vehicle model. X_{ref} denotes the unstable equilibrium point $(0, 0)$ on the ground. The anti-rollover controller determines the lateral tyre force to be generated for reinstating the vehicle. The present study suggests producing the control force calculated by the SDRE-based anti-rollover controller through the control of the wheel steer angle about the kingpin axis (δ_k). Professional ski-stunt driving performers achieve the balancing of the vehicle in the upright position using steering wheel inputs. It proves the steer angle control to be effective in controlling a vehicle at the tip-over point. In a front-wheel steered system, it is possible to control only the steer angles at the front, which restricts a predominant control over the tyre forces generated at rear tyres. In this study, initially, an estimate of the lateral tyre force available on the rear tyre is obtained using a rear tyre's model in the form of a lookup table, as depicted in Figure 19. The block receives values of the slip angle and normal reaction of the rear tyre as inputs. The control input force's remaining value is generated on the front tyre such that the sum of tyre forces on the front and rear tyres results in the control force proposed by the gain-scheduled SDRE controller.

The corresponding value of δ_k to be applied on the front wheel for the generation of tyre force demands attention. The methodology used for the determination of δ_k is described in the next subsection.

Determination of steer angle about kingpin axis

In this study, the appropriate wheel steer angle, δ_k, corresponding to a lateral tyre force to be generated is obtained by inverting the tyre model presented in Figure 18. For all the nonlinear lateral tyre force characteristic curves, it can be seen that the force attains a maximum, then drops, and then remains constant even with an increase in slip angle. The region of the curve until the lateral tyre force attains the maximum is used
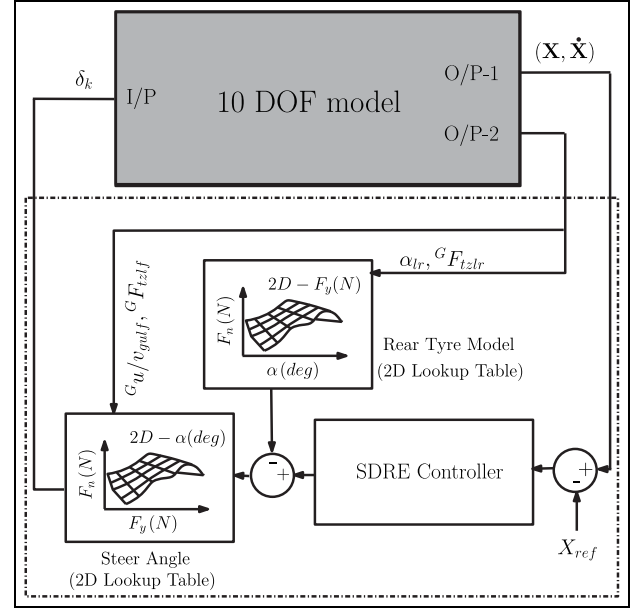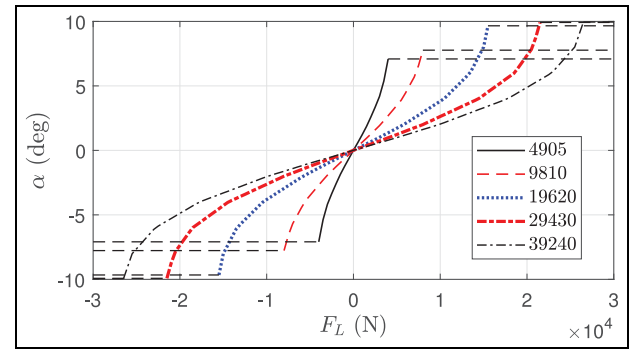
for inversion. The corresponding slip angle is obtained by inverting the tyre model for a particular value of the normal load. If the lateral force is beyond the saturation value, the value of slip angle at the maximum point is used, as any further increase in slip angle would reduce the chance of obtaining higher lateral tyre forces. Figure 20 presents the graph obtained by inverting the tyre model graphs. Any intermediate point is obtained through 2D spline interpolation. Once the slip angle is obtained, the corresponding δ_k can be found from equation (28).

Validation of relaxation of W_{θ_1} for landing phase

The section 'Relaxation of W_{θ_1} for the landing phase' proposed relaxation of weight for the landing phase to limit the control input force to a range which is attainable on the tyres under the existing saturation
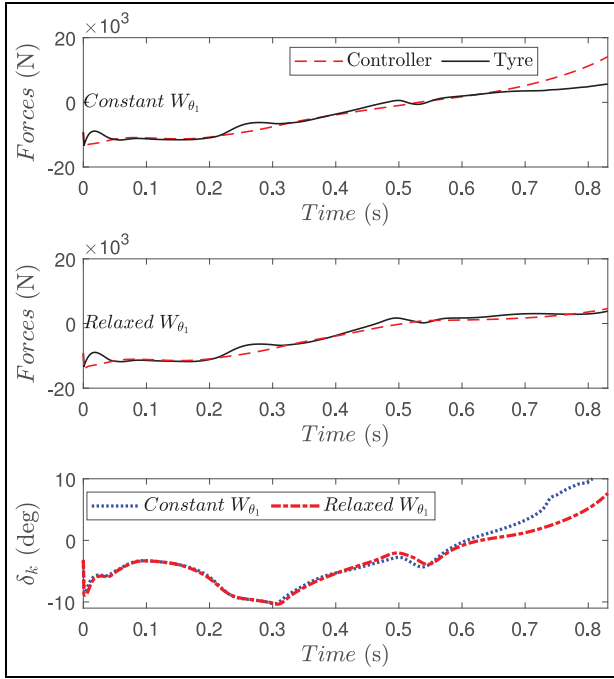
Figure 21. Validation of relaxed W_{θ_1} for landing phase.

Figure 22. Change in roll states of the 10-DOF model.
DOF: degrees of freedom.

conditions. It is validated in this subsection if the reduced control force proposed by the controller due to these relaxed weight values is achievable using wheel steer input. A simulation is conducted using the configuration presented in Figure 19 using the MATLAB®/Simulink® environment. The initial conditions of the 10-DOF model are chosen as $\theta = 0.9788$ rad, $\theta_f = \theta_r = 0.9977$ rad, $\dot{\theta} = 1.2$ rad/s and $\dot{\theta}_f = \dot{\theta}_f = 1.2$ rad/s. These are the equivalent initial conditions of an IDPC model at $\theta_1 = \theta_{1,0}$, $\theta_2 = \theta_{2,0}$ and $\dot{\theta}_1 = 1.2$ rad/s. The constant weight value W_{θ_1} for the recovery phase is chosen as 7000. The variable weight model used is same as presented in Figure 11. Two case studies were conducted. One with a constant weight value W_{θ_1} throughout the simulation and another one with the relaxed weight value for the landing phase. Figure 21 presents results of the case studies.

The vehicle was recovered from the tip-over and brought down to the ground in both cases. Figure 21 also shows the comparison of the forces suggested by the controller and produced on the tyre, on the application of an estimated value of δ_k. The steer angle, δ_k, applied in each case, is also presented in the graph. In the recovery phase, the plots are identical since weight values are the same for both the cases. Whereas in the landing phase, for a constant W_{θ_1} value, the input force proposed by the controller is not achievable even with the application of a higher value of δ_k. But in the relaxed case, the force suggested by the controller is achievable, and a good correlation can be observed between the forces in the landing phase. A similar correlation can be seen in all the case studies presented in the following sections. Hence, the assumptions made are proved to be valid.
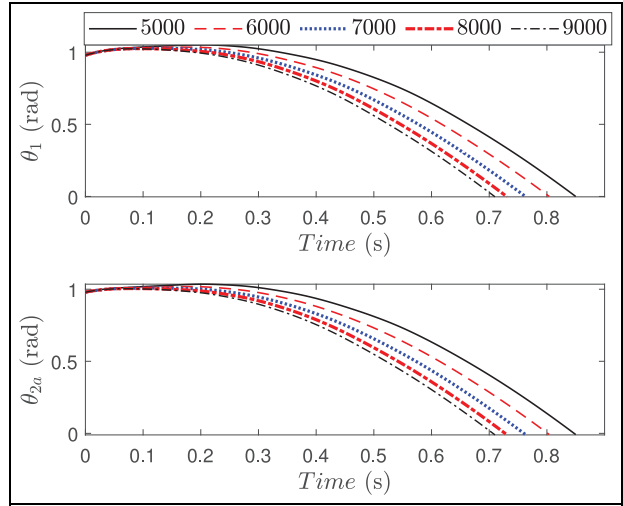
Evaluation of SDRE controller with 10-DOF vehicle model

The present subsection evaluates the 10-DOF full vehicle model with the gain-scheduled SDRE controller using the configuration shown in Figure 19. The initial conditions of the model are assumed as $\theta = 0.9788$ rad, $\theta_f = \theta_r = 0.9977$ rad, $\dot{\theta} = 1.2$ rad/s and $\dot{\theta}_f = \dot{\theta}_f = 1.2$ rad/s. It is the same extreme tip-over scenario used in the previous sections. A constant weight W_{θ_1} is assumed for the recovery phase, and the relaxed W_{θ_1} is used for the landing phase. Various simulations were conducted by varying the weight value W_{θ_1} used for the recovery phase from 5000 to 9000 by keeping the relaxed weights the same. Figure 22 presents the change in roll states of the 10-DOF system in all the case studies.

The state θ of the 10-DOF model is equivalent to θ_1 of the IDPC model. The sprung mass roll angle is presented in absolute scale $\theta_{2a} = (\theta_f + \theta_r)/2$. The vehicle model was reinstated to safety from the tip-over point in all the simulations conducted. The gain-scheduled SDRE anti-rollover controller adequately accounted for the nonlinearities involved in the problem. It performed satisfactorily in the presence of dynamic effects neglected in the controller formulation. The time over which the vehicle was recovered to the ground decreased with an increase in weight value. Figure 23 presents the comparison of force proposed by the controller and produced on the tyres in all the case studies. The corresponding δ_k applied for the generation of the tyre force can be seen in Figure 24. In all the cases, a really good correlation can be found between controller and tyre forces due to the relaxation of weight in the landing phase, as mentioned in the previous section. It is also evident that the force proposed by the controller increased with an increase in weight value.

That justifies the reduction in the recovery time with an increase in weight value. The correlation between
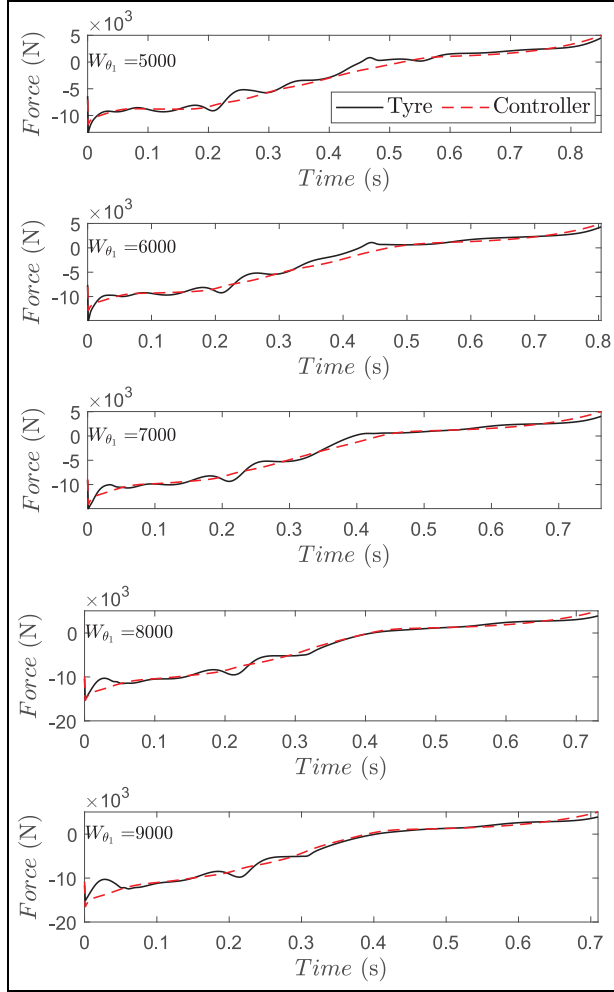
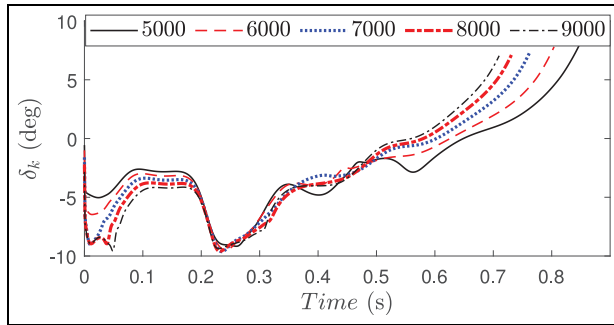**Figure 23.** Controller and tyre forces in each case study.

Figure 24. δ_k obtained in all the case studies.

the forces in the initial time of the recovery phase is of importance. As the weight value increased from 5000 to 9000, the force proposed by the controller increased.

For high values of weight, the corresponding high values of tyre forces were unable to generate even with the application of a higher δ_k for the existing saturation conditions. Hence, the tyre force generated at the initial time of the recovery phase is found to be less than the controller input force. Here, the W_{θ_1} acts as a parameter suitable for the tuning of the controller
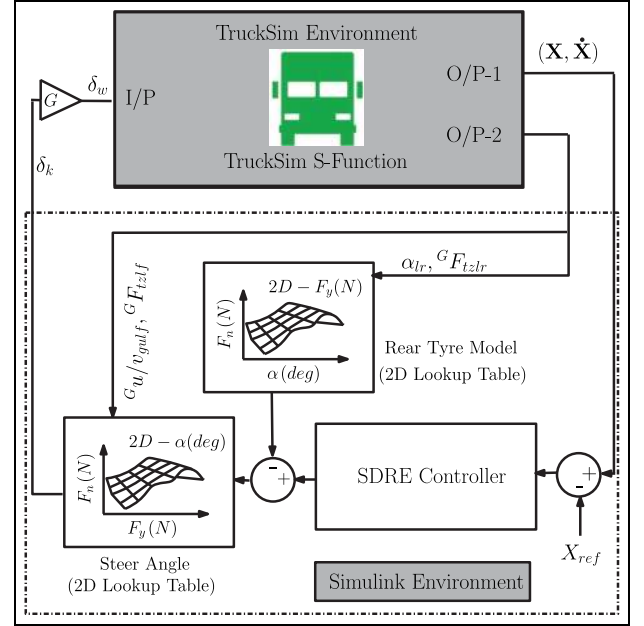

Figure 25. TruckSim® and MATLAB®/Simulink® co-simulation environment.

continuously, unlike in the NMPC method where the terminal matrices or equilibrium points need to be selected differently to obtain various performance points. A good correlation can be found for $W_{\theta_1} = 7000$ in these case studies, and the same value of W_{θ_1} is used for final evaluation in the subsequent section.

Evaluation of SDRE controller with TruckSim® full vehicle model

The preceding section presented the evaluation of the SDRE controller with the 10-DOF full vehicle model. The current section evaluates the gain-scheduled SDRE controller with a highly sophisticated TruckSim® vehicle dynamics model. The software includes comprehensive models of all the vehicle dynamics effects considered by original equipment manufacturers (OEMs). The study makes use of a full-size pick-up truck model with a 5.5 ft long bed. The model has front and rear axle suspension systems with combined slip tyre models. The standard specifications available in the software model are used for the study. Figure 25 presents the layout in which the SDRE controller is applied to the TruckSim® vehicle dynamics model.

The simulation runs in a TruckSim® and MATLAB®/Simulink® co-simulation environment. The vehicle model is present in the TruckSim® environment, and the controller is implemented in the Simulink® environment. During the simulation, both these environments continuously exchange data with each other, giving rise to the co-simulation environment. The SDRE controller and subsystems enclosed in the dotted box perform the same way as described in
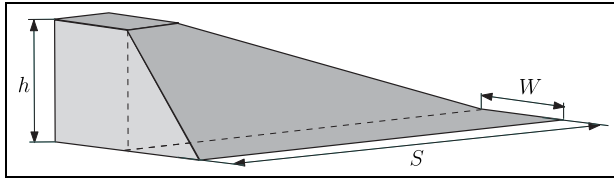
Figure 26. Specifications of the bump.

Figure 27. Simulation that resulted in a rollover.

the previous section using Figure 19. This subsystem is implemented in Simulink® environment. The O/P-1 and O/P-2 nodes also contain the same set of measurements as described in Figure 19. During the simulation, these outputs are obtained from TruckSim® and transferred to Simulink® environment through the built-in interface. It was already mentioned in the previous descriptions that the output of the control system is the steer angle, δ_k. In this study, the proposed δ_k is obtained by controlling the steering wheel angle (δ_w) at the driver's end. Ackerman steering system with a nominal steering gear ratio (G) of 25 available in the TruckSim® environment is used as the steering subsystem. Tie rod and steering column compliances of the steering system are 6×10^{-4} and 1×10^{-4} deg/Nm, respectively. The steering mechanism can make use of advanced systems to improve the accuracy of the wheel steer angle applied in these high-speed critical situations.[34,35] The proposed controller values can also be obtained using an active steer system, which can be made independent of the driver's input by using a planetary gear system. There are steering mechanisms available which can even independently control each wheel on an axle.[36]

It must be noted that the analytical IDPC vehicle model and the 10-DOF full vehicle model make use of initial conditions at the tip-over point with a severe roll rate. The TruckSim® vehicle dynamic software creates real-life simulations, and the initial conditions are not of choice but should be generated through simulations. The rollover scenarios of a vehicle moving at high speeds on a highway can either be manoeuvre induced or due to tripping. Performing an extreme manoeuvre like high-speed collision avoidance can induce an untripped rollover. An example of a tripped rollover is when the vehicle encounters a traffic barrier, such as a divider or guard rail. In such an instance, the vehicle has a very high momentum, which makes it climb the traffic barriers, and results in a quick wheel lift-off. In the TruckSim® vehicle model, the initial conditions are obtained through simulations using the bump shown in Figure 26. The bump has three characteristic dimensions, height (h), length (S) and width (W). The entire shape of the bump is produced using linear interpolation and extrapolation from these characteristic dimensions. These characteristic dimensions h, S and W were varied to obtain different initial conditions.

The speed of the vehicle is assumed to be a fixed value of 100 km/h. The proposal is to recover a vehicle
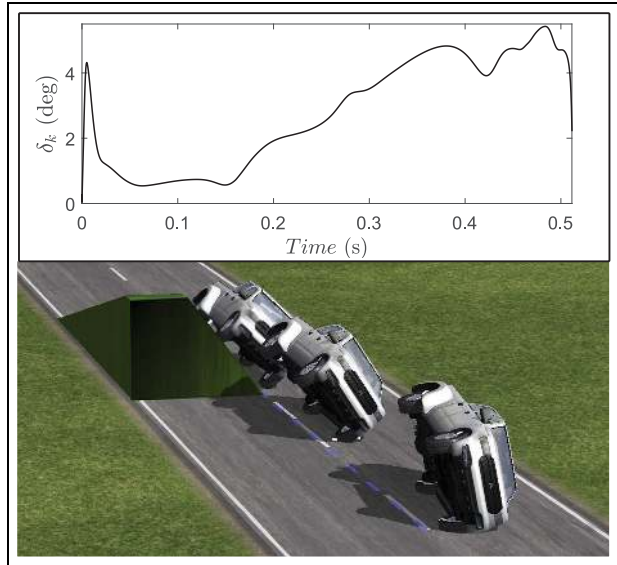
from an on-road high-speed tip-over point. Simulations were attempted for various speeds and bump dimensions. For speeds beyond this range, all the four wheels got lifted off the ground, making the vehicle a projectile. A case where the wheels on either side are lifted off the ground is out of the scope of this study. Hence, throughout this particular study, a fixed speed of 100 km/h is used. It is an on-road simulation, and the friction coefficient is taken as $\mu = 0.85$, which is of dry asphalt.

A simulation is conducted using the bump dimensions $h = 2.5$ m, $S = 15$ m and $W = 2$ m. The weight value is chosen as $W_{\theta_1} = 7000$ for the recovery phase. The duration of time starting from the instant when the vehicle just departs from the bump and starts travelling on two wheels and until the time it touches the ground is considered in these simulations. The initial conditions attained by the vehicle are $\theta_1 = 0.7791$ rad, $\theta_{2a} = 0.7791$ rad, $\dot{\theta}_1 = 0.5518$ rad/s and $\dot{\theta}_{2a} = 1.2527$ rad/s. It must be noted that the simulation is conducted for obtaining a set of tip-over initial conditions, and the same initial conditions can also be obtained from a different set of vehicle speed and bump dimensions. To understand the intensity of the initial condition obtained, a random rollover steer input is given to the vehicle from the initial conditions mentioned above. The rollover steer input given here is merely an inversion of the recovery steer angle proposed by the SDRE controller. The simulation resulted in a rollover, and Figure 27 shows the simulation scenario.

It proves that the initial conditions produced in the simulation are intense enough that in a panic situation, a rollover steer input from an inexperienced driver may result in a rollover accident. It must also be noted that the tip-over equilibrium points are $\theta_{1,0} = 0.9788$ rad and $\theta_{2a,0} = 0.9976$ rad, and the initial conditions mentioned here are not too close to them and yet the
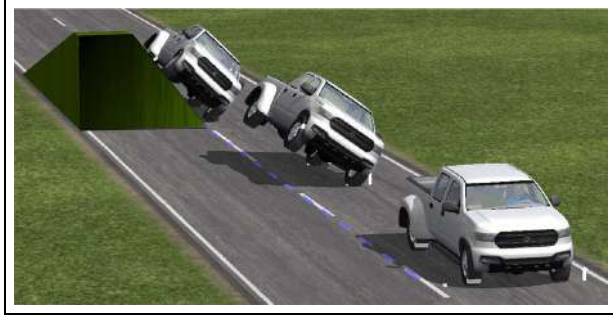
Figure 28. Recovery of TruckSim® vehicle dynamics model.

Figure 29. Comparison of control and tyre forces.

simulation resulted in a rollover. Initial conditions that are close to this tip-over point are presented in subsequent sections.

Comparative study of control action of SDRE controller on TruckSim® and 10-DOF full vehicle models

It was stated before that the TruckSim® model is very sophisticated, and the SDRE controller must be evaluated with it to understand the performance of the same in real-life scenarios with actual initial conditions. At the same time, a rigorous evaluation of the gain-scheduled SDRE controller was conducted in the previous section using the 10-DOF full vehicle model. The 10-DOF model was preferred due to the convenience of setting up initial conditions as well as performing simulations. It is essential to compare the control action of the gain-scheduled SDRE controller on 10-DOF full vehicle model as well as the pick-up truck model obtainable in TruckSim® software. The simulation with the same set of initial conditions $\theta_1 = 0.7791$ rad, $\theta_{2a} = 0.7791$ rad, $\dot{\theta}_1 = 0.5518$ rad/s and $\dot{\theta}_{2a} = 1.2527$ rad/s obtained in the previous section that resulted in a rollover is used here for simulation. Here the vehicle with the same initial conditions was reinstated to the ground using the gain-scheduled SDRE controller in the TruckSim® and MATLAB®/Simulink® co-simulation environment presented in Figure 25. Figure 28 shows the simulation scenario where the vehicle was reinstated from the tip-over point.

To perform a comparative study, the 10-DOF model was initiated from the same initial conditions as the simulation obtained in the TruckSim® setup. The simulation with 10-DOF model was accomplished using the layout exhibited in Figure 19. Figure 29 presents the comparative study between the force proposed by the controller and produced on the tyres in both cases. It can be observed from the graphs that the controller forces suggested in both cases are of comparable magnitude. In the 10-DOF model, the forces proposed by the controller and produced on the tyre follow each other closely, whereas, in the TruckSim® model, the correlation is close, but not as good compared to the previous case. The variation is due to the fact that
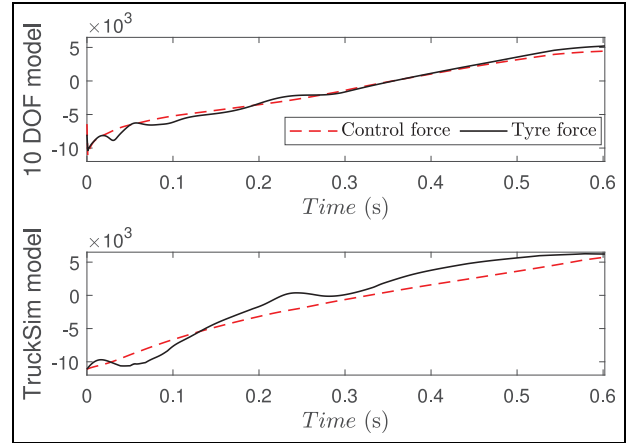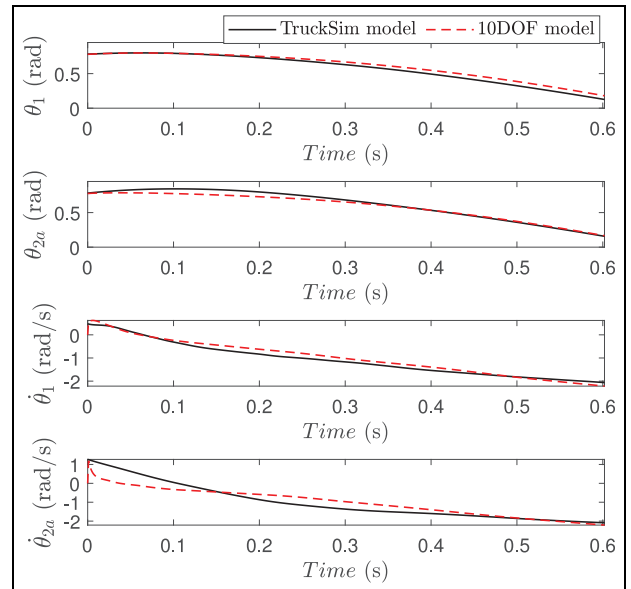

Figure 30. Comparison of roll states of TruckSim® and 10-DOF models.

the TruckSim® pick-up truck model makes use of a combined slip tyre model, unlike the 10-DOF model and also incorporates the effects of steering and suspension geometry.

Figure 30 shows the comparison of change in the roll states between 10-DOF model and TruckSim® model in the simulation study. It is evident from the plots that two of these models were brought down to the ground at comparable times.

The results justify using the analytical 10-DOF full vehicle model to analyse the performance of the gain-scheduled SDRE controller.

Case studies on action of SDRE controller with TruckSim® vehicle dynamics model

This section describes an extensive study of the gain-scheduled SDRE controller with the sophisticated

pick-up truck model obtainable in the TruckSim® software using the TruckSim® and MATLAB®/Simulink® co-simulation environment. Five case studies were conducted with various intensities in terms of the initial conditions. Each set of initial conditions was attained by running the vehicle over the bump depicted in Figure 26. The speed of the vehicle was set to be constant at 100 km/h, as mentioned before. The width W and length S of the bump were set to be 2 and 30 m, respectively, for all the case studies. The value of height h was varied to obtain various initial conditions, and the values used in the case studies presented in this section are 2.8, 2.9, 2.95, 3 and 3.2 m. Figure 31 presents the change in roll states of the system with time for all the case studies conducted.

It is evident that as the height of the bump increased, the intensity of the initial conditions obtained increased from Case 1 to Case 5. Case 1 presents the least intense initial conditions in terms of roll states and the values are $\theta_1 = 0.7058$ rad, $\theta_{2a} = 0.7159$ rad, $\dot{\theta}_1 = 0.8847$ rad/s and $\dot{\theta}_{2a} = 1.4396$ rad/s. The most intense set of initial conditions are obtained in Case 5 and the initial conditions are $\theta_1 = 0.9574$ rad, $\theta_{2a} = 0.9673$ rad, $\dot{\theta}_1 = 1.3090$ rad/s and $\dot{\theta}_{2a} = 1.7068$ rad/s. In Case 5, starting from the above-mentioned initial conditions, the vehicle attained the maximum values of roll angles $\theta_1 = 0.9762$ rad and $\theta_{2a} = 1.0640$ rad during the recovery action which is higher than the unstable equilibrium point $(\theta_{1,0}, \theta_{2,0})$ at the tip-over point. The vehicle was successfully reinstated from the tip-over scenario in all the case studies conducted. Figure 32 presents the simulation scenario in the MATLAB®/Simulink® co-simulation environment for the most intense case, that is, Case 5.

Figure 33 presents the comparison between the force recommended by the controller and the corresponding force produced on the tyres by the application of δ_k. It can be seen that as the intensity increased from Case 1 to Case 5, the control input force required to reinstate the vehicle increased. It has already been mentioned that the initial conditions were generated by driving the vehicle over the bump. As the intensity of the initial conditions increased, at the time the vehicle left the bump, along with the wheels on the right side, the wheel at the front left corner as well tended to lift-off. In such cases, the values of the roll states at the moment the front left wheel touched the ground were taken as the initial conditions.

This produced a bouncing effect during the control action. There was a slight increase in the forward slip ratio at this initial phase, and it, in turn, produced a tyre force higher than anticipated. On the contrary, as the simulation proceeded further, the normal reaction reduced as the tyres bounced back after this initial effect. It resulted in the generation of a lower tyre force at one point in the later stage of the simulation than anticipated. This effect appeared to be higher in intense initial conditions such as Case 5. Figure 34 presents the steer angle, δ_k, applied in each case study. In all the
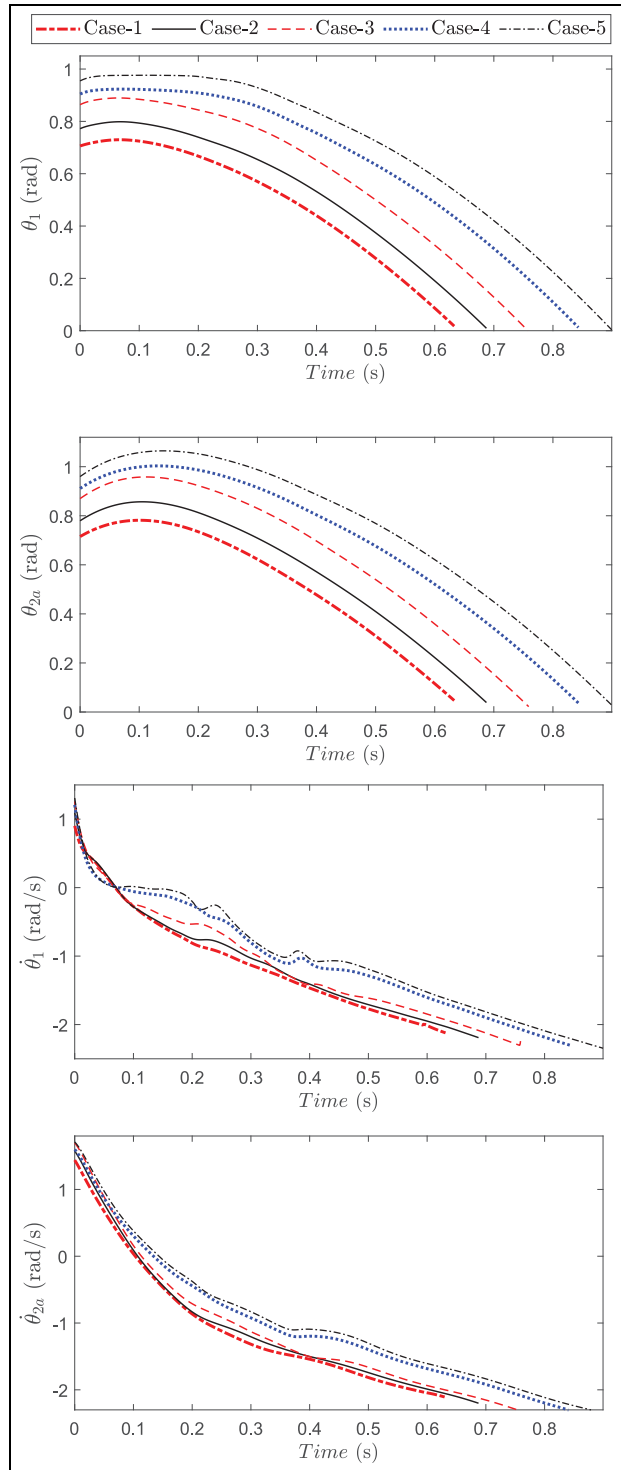
Figure 31. Change in roll states in all the case studies.

case studies presented, the δ_k is well within the range that can be achieved in a real-life scenario. The gain-scheduled anti-rollover controller accounted for the nonlinearities involved in the problem adequately well. The controller performed satisfactorily in the presence of all the dominant dynamic effects relevant in a real-life simulation scenario. The 2D gain-scheduling employed in this study significantly reduced the computation time per sample, making it suitable for real-time implementation.

Figure 32. Recovery action performed in Case 5.

Figure 34. Variation of δ_k in all the case studies.

Figure 33. Control and tyre forces obtained in case studies.

Conclusion

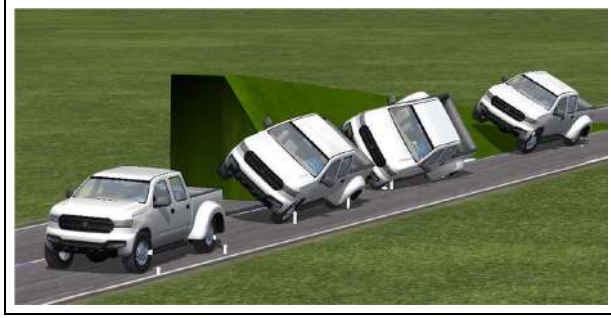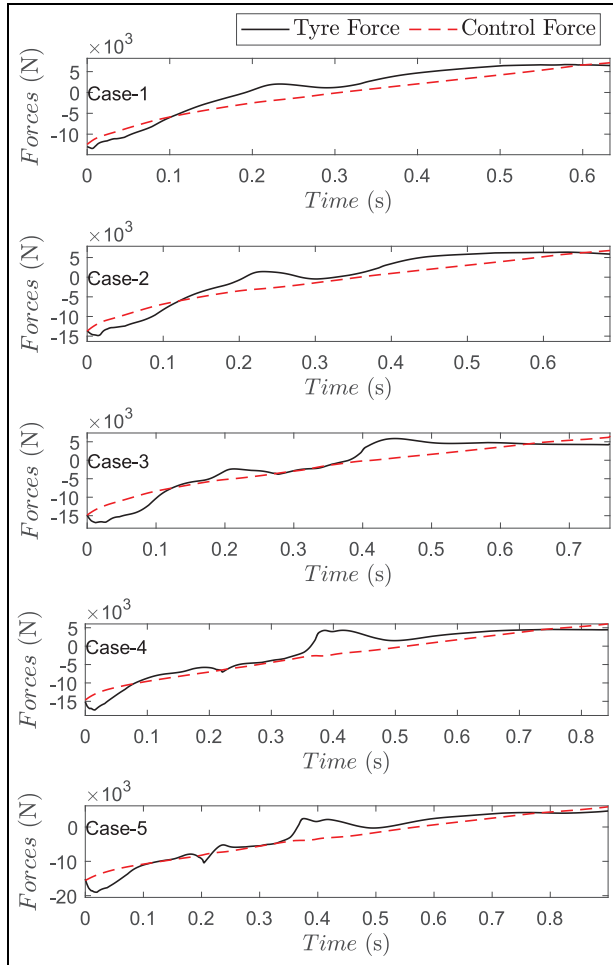The study proposed a novel gain-scheduled SDRE-based optimal anti-rollover controller to reinstate a vehicle from a tip-over point. The design methodology made use of an IDPC vehicle model with a virtual rollover torque instead of the gravity torque as the plant model. The introduction of the virtual rollover torque eliminated the unstable equilibrium point at the tip-over point and acted as an easy solution for generating an equilibrium point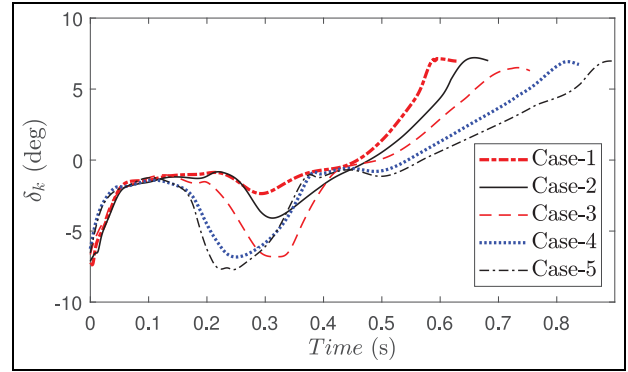 on the ground. The controller's evaluation with the real IDPC vehicle model with gravity torque proved it to be effective in reinstating a vehicle at the near tip-over point. It was able to adjust the magnitude of the control input using the weight value corresponding to the vehicle's roll motion (W_{θ_1}) through the coupling that exists across the cost values of state variables and control input force in the performance index. The weight value was identified as an effective tool for continuously tuning the performance of the SDRE controller. In the landing phase, the vehicle model achieved a high value of vehicle roll rates. Consequently, the normal reaction forces dropped readily in the landing phase. The dedicated strategy incorporated in the controller for the landing phase was found to be effective in varying the controller's weight value depending on the roll rate achieved by the vehicle to keep the control input force within the saturation limit. The SDRE controller formulation has specific state dependencies and can be presented as a 2D gain-scheduled controller. The gain-scheduling eliminated the need to solve the nonlinear optimal control problem in real time, allowing the use of a 2D lookup table instead. The computation time per sample of the resulting gain-scheduled SDRE controller in MATLAB® was found to be in the order of 10^{-2} s only. An evaluation of the SDRE anti-rollover controller with the 10-DOF full vehicle model with a nonlinear pure slip model was conducted. The study proved the anti-rollover controller to be effective in the presence of dynamic effects, which were neglected during the controller formulation using the reduced-order IDPC vehicle model. The SDRE-based optimal controller adequately accounted for the complex nonlinearities involved in the nature of the vehicle model. The wheel steer angle associated with the SDRE controller obtained by the inversion of the nonlinear pure slip tyre model provided a good correlation between the control input and the force tyre forces. The performance of the proposed gain-scheduled SDRE anti-rollover controller is validated with the real-life simulation software TruckSim® along with the MATLAB®/Simulink® co-simulation environment for various initial conditions. The anti-rollover was found to be effective in reinstating the sophisticated

TruckSim® pick-up model from different intense near tip-over scenarios considered for the study. The scope of future work includes the use of a better normal reaction force prediction model to understand the saturation force limit in existence. A new wheel steer angle model that incorporates a combined slip tyre model can give a better correlation between controller and tyre forces. A study on the choice of an optimal virtual rollover torque characteristic is also within the scope of future research.

Declaration of conflicting interests

The author(s) declared no potential conflicts of interest with respect to the research, authorship, and/or publication of this article.

Funding

ORCID iD

Hari M Nair https://orcid.org/0000-0003-0013-8512

References

1. Singh K. *Road accidents in India – 2017*. New Delhi, India: Ministry of Road Transport and Highways Transport Research Wing, Government of India, 2018, www.morth.nic.in

2. National Highway Traffic Safety Administration. Rollover, https://www.safercar.gov/Vehicle-Shoppers/Rollover (accessed 20 January 2020).

3. Nair H and Sujatha C. A new rollover detection system for tripped and untripped rollovers for antiroll safety systems. In: *19th international and 14th European-African regional conference of the ISTVS*, Budapest, Hungary, 25–27 September 2017, pp.1–8. Ferrara: ISTVS.

4. Phanomchoeng G and Rajamani R. New rollover index for the detection of tripped and untripped rollovers. *IEEE T Ind Electron* 2012; 60: 4726–4736.

5. Yoon J, Kim D and Yi K. Design of a rollover index-based vehicle stability control scheme. *Vehicle Syst Dyn* 2007; 45: 459–475.

6. Dahlberg E. *Commercial vehicle stability – focusing on rollover*. PhD Thesis, Institutionen för farkostteknik, Stockholm, 2001.

7. Chen BC and Peng H. Differential-braking-based rollover prevention for sport utility vehicles with human-in-the-loop evaluations. *Vehicle Syst Dyn* 2001; 36: 359–389.

8. Kang J, Yoo J and Yi K. Driving control algorithm for maneuverability, lateral stability, and rollover prevention of 4wd electric vehicles with independently driven front and rear wheels. *IEEE T Veh Technol* 2011; 60: 2987–3001.

9. Shao K, Zheng J and Huang K. Robust active steering control for vehicle rollover prevention. *Int J Model Identif Contr* 2019; 32: 70–84.

10. Parida NC, Raha S and Ramani A. Rollover-preventive force synthesis at active suspensions in a vehicle performing a severe maneuver with wheels lifted off. *IEEE T Intell Transp* 2014; 15: 2583–2594.

11. Vu VT, Sename O, Dugard L, et al. Active anti-roll bar control using electronic servo valve hydraulic damper on single unit heavy vehicle. *IFAC PapersOnline* 2016; 49: 418–425.

12. Peters SC, Bobrow JE and Iagnemma K. Stabilizing a vehicle near rollover: An analogy to cart-pole stabilization. In: *IEEE international conference on robotics and automation*, Anchorage, AK, 3–7 May 2010, pp.5194–5200. New York: IEEE.

13. Jaiwat P and Ohtsuka T. Stabilization of suspension vehicle near rollover by nonlinear model predictive control. *SICE J Contr Meas Syst Integr* 2014; 7: 364–373.

14. Jaiwat P and Ohtsuka T. Recovery of vehicle near rollover by nonlinear model predictive control. *SICE J Contr Meas Syst Integr* 2015; 8: 380–389.

15. Lan JT. *Tip-up and stabilization of an autonomous four-wheeled vehicle*. PhD Thesis, Massachusetts Institute of Technology, Cambridge, MA, 2011.

16. Zhong W and Rock H. Energy and passivity based control of the double inverted pendulum on a cart. In: *Proceedings of the 2001 IEEE international conference on control applications (CCA'01)* (Cat. No. 01CH37204), Mexico City, 7 September 2001, pp.896–901. New York: IEEE.

17. Xin X. Analysis of the energy-based swing-up control for the double pendulum on a cart. *Int J Robust Nonlin* 2011; 21: 387–403.

18. Nair HM and Sujatha C. Prevention of vehicle rollover after wheel lift-off using energy-based controller with proportional gain augmentation. *Proc IMechE, Part D: J Automobile Engineering* 2020; 234: 963–980.

19. Alirezaei M, Kanarachos S, Scheepers B, et al. Experimental evaluation of optimal vehicle dynamic control based on the State Dependent Riccati Equation technique. In: *2013 American control conference*, Washington, DC, 17–19 June 2013, pp. 408–412. New York: IEEE.

20. Acarman T. Nonlinear optimal integrated vehicle control using individual braking torque and steering angle with online control allocation by using State-Dependent Riccati Equation technique. *Vehicle Syst Dyn* 2009; 47: 155–177.

21. Madhusudhanan AK, Corno M, Bonsen B, et al. Solving algebraic Riccati equation real time for integrated vehicle dynamics control. In: *2012 American control conference (ACC)*, Montreal, QC, Canada, 27–29 June 2012, pp.3593–3598. New York: IEEE.

22. Mohammadi SS and Khaloozadeh H. Optimal motion planning of unmanned ground vehicle using SDRE controller in the presence of obstacles. In: *2016 4th international conference on control, instrumentation, and automation (ICCIA)*, Qazvin, Iran, 27–28 January 2016, pp.167–171. New York: IEEE.

23. Ikeda Y. Active steering control of vehicle by sliding mode control-switching function design using SDRE. In: *2010 IEEE international conference on control applications*, Yokohama, Japan, 8–10 September 2010, pp.1660–1665. New York: IEEE.

24. Villagra J, d'Andrea-Novel B, Mounier H, et al. Flatness-based vehicle steering control strategy with SDRE feedback gains tuned via a sensitivity approach. *IEEE T Contr Syst T* 2007; 15: 554–565.

25. Wachter E. *Lateral path tracking in limit handling condition using SDRE control*. Ghotenburg: Department of Applied Mechanics, Chalmers University of Technology, 2016.

26. Bogdanov A. *Optimal control of a double inverted pendulum on a cart*. Technical Report CSE-04-006. Beaverton, OR: OGI School of Science and Engineering, Oregon Health and Science University, 2004.

27. Dang P and Lewis FL. Controller for swing-up and balance of single inverted pendulum using SDRE-based solution. In: *31st annual conference of IEEE Industrial Electronics Society, 2005 (IECON 2005)*, Raleigh, NC, 6–10 November 2005, pp.304–309. New York: IEEE.

28. Kim S and Kwon S. Nonlinear optimal control design for underactuated two-wheeled inverted pendulum mobile platform. *IEEE-ASME T Mech* 2017; 22: 2803–2808.

29. Erdem EB and Alleyne AG. Experimental real-time SDRE control of an underactuated robot. In: *Proceedings of the 40th IEEE conference on decision and control* (Cat. No. 01CH37228), vol. 3, Orlando, FL, 4–7 December 2001, pp.2986–2991. New York: IEEE.

30. TruckSim®, Mechanical Simulation Corporation, www.carsim.com/products/trucksim/ (accessed 2 February 2020).

31. Nair HM and Chandramohan S. Vehicle tip-over prevention using SDRE controller. In: *6th international conference on control, automation and robotics (ICCAR)*, Singapore, 20–23 April 2020, pp.404–408. New York: IEEE.

32. Bakker E, Nyborg L and Pacejka HB. Tyre modelling for use in vehicle dynamics studies. *SAE technical paper* 870421, 1987.

33. Cimen T. Systematic and effective design of nonlinear feedback controllers via the State-Dependent Riccati Equation (SDRE) method. *Annu Rev Control* 2010; 34: 32–51.

34. Zhao W, Fan M, Wang C, et al. H/extension stability control of automotive active front steering system. *Mech Syst Signal Pr* 2019; 115: 621–636.

35. Zhao W, Zhang H and Li Y. Displacement and force coupling control design for automotive active front steering system. *Mech Syst Signal Pr* 2018; 106: 76–93.

36. Ahmed A, Rawat V and Bhat R. Vehicle steering mechanism for active independent front steering system. In: *3rd international conference on mechanical, production and automobile engineering (ICMPAE'2013)*, Bali, Indonesia, 4–5 January 2013, pp.83–85, http://psrcentre.org/images/extraimages/17.%20113126.pdf

Appendix 1

Table 2. Specifications of the 10-DOF model.

Notation	Value
a	1.4 m
b	2.88 m
b_{slf}, b_{srf}	1×10^4 Ns/m
b_{slr}, b_{srr}	1.5×10^4 Ns/m
c_f	1.75 m
c_r	1.90 m
J_x	846.5 kg m^2
J_{xf}	80 kg m^2
J_{xr}	205 kg m^2
J_y	5757 kg m^2
J_z	5757 kg m^2
k_{slf}, k_{srf}	1.5×10^5 N/m
k_{slr}, k_{srr}	2.5×10^5 N/m
k_{tlf}, k_{trf}	7.5×10^5 N/m
k_{tlr}, k_{trr}	7.5×10^5 N/m
l_0	0.416 m
m	2000 kg
m_f	210 kg
m_r	530 kg
m_t	2740 kg
r_0	0.435 m

DOF: degrees of freedom.

Appendix 2

Table 3. Notation.

Symbol	Description
a	Distance of CG from front axle
$\overline{\mathbf{A}}, \overline{\mathbf{B}}, \mathbf{D}, \mathbf{E}$	SDC matrices of the IDPC model
$\mathbf{B}, \mathbf{C}, \mathbf{H}, \mathbf{P}$	Coefficient matrices of the IDPC vehicle model
b	Distance of CG from rear axle
b_s	Damping coefficient
b_l	Linear damping (IDPC)
c_f	Track width at front
c_r	Track width at rear
$\overline{\mathbf{D}}, \mathbf{D}^\star$	Weight matrices in the performance index
F_L	Lateral tyre force
F_n	Normal reaction force
F_s	Suspension force
F_{tx}, F_{ty}, F_{tz}	Tyre forces
$^G()$	Physical quantities in ground coordinate system
G	Gear ratio of the steering mechanism
g	Acceleration due to gravity
h, S, W	Height, length and width of the bump
i	Index corresponding to left (l) or right (r)
j	Index corresponding to front (f) or rear (r)
J_x	Roll inertia
J_{xf}	Roll inertia of front axle
J_{xr}	Roll inertia of rear axle
J_y	Pitch inertia
J_z	Yaw inertia
J_1	Roll inertia of unsprung mass (IDPC)
J_2	Roll inertia of sprung mass (IDPC)
k_s	Suspension stiffness
k_t	Tyre stiffness
k_l	Linear stiffness (IDPC)
k_5	Fifth-order stiffness (IDPC)

(continued)

Table 3. Continued

Symbol	Description
l	Instantaneous length of the suspension
l_1	Axle-link length (IDPC)
l_2	Sprung mass-link length (IDPC)
l_0	Initial length of the suspension
m	Sprung mass
m_f	Unsprung mass at front
m_r	Unsprung mass at rear
m_t	Total mass of the vehicle
m_1	Sprung mass (IDPC)
m_2	Unsprung mass (IDPC)
$\mathbf{P}^\star$	Virtual rollover torque and spring forces
$\mathbf{q}, \dot{\mathbf{q}}, \mathbf{q}$	DOF of the IDPC vehicle model
r	Instantaneous radius of the tyre
r_0	Initial radius of the tyre
$^s()$	Physical quantities in sprung mass coordinate system
$^T()$	Physical quantities in tyre coordinate system
u	Longitudinal speed
u_{cs}, v_{cs}, w_{cs}	Corner velocities of the sprung mass
u_{cu}, v_{cu}, w_{cu}	Corner velocities of the unsprung mass
u_f	Longitudinal speed of front axle
u_{gu}, v_{gu}	Velocities at tyre–road contact point
u_r	Longitudinal speed of rear axle
v	Lateral speed
v_f	Lateral speed of front axle
v_r	Lateral speed of rear axle
w	Vertical speed
w_f	Vertical speed of front axle
w_r	Vertical speed of rear axle
x_s	Suspension deflection
x_t	Tyre deflection
$\mathbf{X}$	State variables of the IDPC model
y	Lateral motion of the vehicle model
α	Slip angle
γ	Pitch angle
δ_k	Steer angle about the kingpin axis
δ_w	Steering wheel angle
θ	Roll angle
θ_0	Axle angle offset (IDPC)
θ_1	Roll motion of the vehicle
θ_2	Relative roll motion of the sprung mass
θ_{2a}	Absolute roll motion of the sprung mass
θ_f	Roll angle of front axle
θ_r	Roll angle of rear axle
τ	Suspension spring force
τ_g	Gravitational torque
τ_{vr}	Virtual rollover torque
ψ	Yaw angle
ω_x	Roll rate
ω_{xf}	Roll rate of front axle
ω_{xr}	Roll rate of rear axle
ω_y	Pitch rate
ω_z	Yaw rate

CG: centre of gravity; DOF: degrees of freedom; IDPC: inverted double pendulum on a massless cart.